UiT The Arctic University of Norway

Faculty of Science and Technology,
Department of Physics and Technology

Solar Photovoltaic Potential on Commercial Buildings in Arctic Latitudes

Andreas Larsen
EOM-3901 Master's thesis in Energy, Climate and Environment
June 2022

UiT The Arctic University of Norway

Abstract

This thesis desires to study the use of solar resources in a less frequently used location, by exploring the use of a photovoltaic systems on the roof of a warehouse in Tromsø, Norway. The research is gathered using a 15 000 $m2$ warehouse as the location, which has an annual energy consumption of 2,9 GWh. The solar resources at this location are highly dependent on season, with periods of polar nights during winter and midnight sun during summer. With this in mind this study considers solar radiation conditions, area utilization and energy production for three photovoltaic systems to find the optimal system for harvesting energy under the mention constraints. The three systems evaluated consists of horizontal modules, 40° tilted south orientated modules and 40° tilted east-west orientated modules, and their energy production respectively covers 16%, 16% and 25% of the warehouse consumption.

Being capable of producing the most energy, system design and an economic analysis is performed for the system with 40° tilted east-west orientated modules. The system consists of 3456 modules with a combined power of 1382 kWp, requires an investment cost of 5 961 000 NOK and breaks even with an electricity price of 0,38 NOK/kWh. In the pursuit of relieving stress from the grid and decreasing the washhouse's electricity cost, this study also investigates the idea of utilizing otherwise unused roofs on neighbour buildings for solar energy production and transmit the energy to the warehouse with inter-building cables. Two building were considered, one closer but limited in size, and one larger in size but further away. Results prove the short inter-building distance to be most profitable when electricity prices are below 0,9 NOK/kWh, due to lower investment costs. For prices above 0,9 NOK/kWh, the extra cost of the longer distance would be more profitable due to the possibility of a larger production area.

Acknowledgements

First, I would thank Professor Matteo Chiesa for exceptional supervision during the period of my work on the thesis. Through both inspiring and creative discussions, he has been a major support in evolving my initial idea into the end-result that forms this thesis. His ability to solve my questions by using creative mindset has been both motivating and educational to experience.

I would also express my gratitude to Coop Norge, represented by Roald Nilsen, for their cooperation during this period. By providing power consumption data to this study and allowing me to inspect their building, Coop has proved to be a supportive company. Several kind people have helped forming this thesis thorough pleasant discussions during the last months. Specially, I would like to thank Ronald Jann Hardersen and Helge Engebø for sharing their knowledge and ideas, I genuinely appreciate the support they have given me. Also, I would like to thank my classmates for contributing to a wonderful time through all my years as a student, their company has been a pleasure both on and off campus. My appreciations also go to the personnel at UiT for their help and support during all years of my education.

As a student staying away from home, I would sincerely thank my family and friends for the time and effort they have put in giving me relaxation through countless of enjoyable moments during my travels home. A special thanks to my dear fiancée Ingrid Støtvig for her endless support during all my time as a student. Her ability to light up my everyday life is deeply appreciated. Finally, I would like to express my gratitude to former colleague Svein Bellmann for his support. During our time together as powerline workers, he gave me a deeper understanding in the theoretical aspects considering our profession which woken my interests in further education.

List of Contents

List of Figures

List of Tables

Abbreviations

ASR	Area Solar Radiation
AC	Alternating Current
C+B1	Coop and Building 1
C+B2	Coop and Building 2
CCC	Current Carrying Capacity
DC	Direct Current
GWh	Gigawatt- hour
HD_m	Height Difference of a Module
HM	Horizontal Modules
kWh	Kilowatt- hour
MPP	Maximum Power Point
MPPT	Maximum Power Point Tracking
NPV	Net Present Value
NVE	Norges Vassdrags- og Energidirketorat
PR	Performance Ratio
PV	Photovoltaics
S_{mr}	Spacing per Module Row
STC	Standard Test Conditions
TEWM	40° Tilted, East- West orientated Modules
TSM	40° Tilted, South orientated Modules
V	Volt
WACC	Weighted Average Cost of Capital
W_r	Row Width

Nomenclature

Symbol	Description	SI-Unit
A	Area	m^2
b	Length Factor (Dimensionless Unit)	1
I	Electric Current	A
L_{cable}	Length, Cable	m
n_c	Cell Efficiency (Dimensionless Unit)	1
n_{ref}	Reference Efficiency (Dimensionless Unit)	1
$n_{string,max}$	String Size (Dimensionless Unit)	1
S	Irradiance	W/m^2
T_c	Temperature, Cell	K
T	Temperature	K
T_{ref}	Temperature, Reference	K
T_{STC}	Temperature, Standard Test Condition	K
Tk_{Voc}	Temperature Coefficient, Open Circuit Volage	$1/K$
V_{OC}	Voltage, Open Circuit	V
$V_{inverter}$	Voltage, Inverter Input	V
V_{MPP}	Voltage, Maximum Power Point	V
ΔV	Change in Voltage	V
W	Power (Watt)	W
α	Solar Elevation Angle (Dimensionless Unit)	1
θ	Angle Between Module and Horizontal (Dimensionless Unit)	1
β_{ref}	Temperature Coefficient (Dimensionless Unit)	1
ρ	Conductor Resistivity	Ohm

1 Introduction

1.1 Background

During the last two decades, the Norwegian energy consumption has increased by 14,6%. A further rise is predicted as the ever- increasing need for decarbonizing our community is aided by electrification of fossil fuel processes. Equinor's desire to electrify their gas plant "Melkøya" in Finnmark within 2027 is one among various examples where electrification of existing industries in Norway is planned (Klo, 2021). Establishments of energy consuming industries are also predicted, as Norway offers industries a sustainable production provided by cheap, renewable energy (Kalkenberg, 2021). Electrification of private households is also predicted to contribute to the increased power consumption. Since 2016, more than 300 000 additional electric vehicles are used as private households' desires to electrify their means of transport (Energi Norge, 2021). Due to the electrification of our society, the power consumption is estimated to have a further growth of 20- 30% during the next decade, increasing Norway's annual electricity demand by of 30- 50 TWh (Holmefjord & Kringstad, 2019).

Such growth gives an additional pressure to the grid in terms of power transmission capacity, as experienced at the Norwegian island Senja where power blackouts frequently occur as a result of power consuming industries overloading the grid. Due to the remote location, expanding the grid is an expensive measure that proves difficult to implement. A solution to this, and similar problems, may be to utilize the energy generation from solar resources to relieving parts of the increased consumption from the grid. In certain parts of the world this development has successfully been implemented, such as in the Persian Gulf region, where more than 7 GW of utility scale photovoltaic (PV) systems have been ordered in less than a decade. The regions commitment to large utility- scale PV systems have resulted in decreased prices in a global scale, leading way for remaining parts of the world to increase the amount of locally produced electricity (Chiesa, Apostoleris, & Ghaferi, 2021).

Likely to have been inspired by this development, the Norwegian food chain Coop has invested in a utility scale system on their main warehouse in Jessheim, Norway, with the objective of creating an energy positive building, producing more energy than it consumes. The system consists of 8270 modules that covers an area of $25\,000\ m^2$ and provides an annual energy production of 2,85 GWh. The system of east- west orientated modules is presented in Figure 1 (Teknisk Ukeblad, 2021).

Figure 1: East- west orientated PV system with an annual power production of 2,85 GWh installed on the roof of Coops main warehouse in Jessheim, Norway (Teknisk Ukeblad, 2021).

1.2 Idea and Purpose

The idea for the subject in this study occurred as author is a former employee at Coop's warehouse in Tromsø and became aware of the buildings major impact on the grid during working hours. This inspired exploring measures for improvements, and the idea was raised of utilizing the unused area on the roof for electricity generation. In addition, a cooperation with Coop seemed interesting as the food- chain proves to be a forward-looking company according to their former investments of utility scale PV systems in Southern Norway.

This study desires to put attention to a less frequent location in terms of solar resources, by investigating the use of a PV system on the roof of a warehouse owned by Coop in Tromsø, Norway. Both electricity prices and power consumption are predicted to rise in the region, using

solar resources to decrease energy cost and relieve the grid is a measure worth investigating. Despite the achievements in the Persian Gulf may positively affect the profitability for utilizing solar resources in Tromsø, the latter is exposed to an additional challenge due to highly seasonal solar availability (Chiesa, et al., 2020). To ensure harvesting the most radiation under the mentioned constraints, three PV systems are evaluated to find the most suited. Solar radiation conditions, area utilization and energy production for the systems are investigated, as well as an economic analysis to determine the most profitable system. The investigation takes place on a 15 000 m^2 warehouse which mainly due to temperature regulation, charging of forklifts, and lightning has an annual energy consumption of 2,9 GWh. This corresponds to the average electricity demand for 180 household. By supplying parts of the warehouse power consumption with energy from solar resources the local grid will be significantly relieved (Energifakta Norge, 2021).

In the pursuit of relieving stress from the grid and decrease Coops electricity cost, this study also investigates the idea of utilizing otherwise unused roofs on neighbour buildings for solar energy production and transmit the energy to Coop using inter- building cables. This idea came up through discussions between Professor Matteo Chiesa and author, as both had the desire for covering an even greater part of Coops power consumption by solar resources without interrupting existing land use. By considering the number of empty roofs surrounding the warehouse with similarities in both orientation and size, the idea seemed feasible. It is likely that such investigation serves purpose further than this study, as similar situations frequently occur in industrial fields, providing additional motivation for investigation. To determine which affect the most, inter- building distance or available roof area, two buildings with differences in the mentioned properties are considered for installing PV systems.

1.3 Limitations

When calculating the electricity production for the PV systems, the module efficiency is assumed to be constant, despite eventual temperature- efficiency correlations. Due to objects such as pipes and fans on the roof, the available area for module installation is assumed to consist of three columns located with proper distances to the mention objects. Further utilization of additional areas on the roof or the walls are not considered. Information given by the warehouse owners suggests that strong winds historically lead to insignificant amounts of snow

on the roof. Therefore, mechanical loads and shadowing caused by snow will not be considered. Despite prices for the module fundaments are utilized in the economic analysis, this study does not perform further investigations on the mentioned component. As the warehouse roof is assumed to handle the weight from the PV system, no further investigations are done regarding the mechanical impact from the PV system on the warehouse roof.

The exact price for the PV systems is unknown as wholesalers in general offers individual agreements based on customer relationships. As changes in the discount rate highly affects the profitability of the project, deviations from the calculated system cost are likely to occur. As this study does not intend to go into depth in researching future electricity prices, a constant electricity price predicted by NVE is assumed for all the three decades of project duration, despite this rate is affected by various factors such as the climate, and both domestic and foreign politics. Whereas the total electricity cost and various details are provided by Coop, certain parts are unavailable, such as price rates for grid rent and consumer fees. To present the complete electricity cost in Table 15, remaining price rates either assumed or collected from the grid supplier Arva. Note that Coop may have an individual agreement with the grid supplier.

1.4 Structure of Thesis

Chapter 2 describes the theoretical background used as a fundament in this thesis, starting with presenting the location in which this study focuses it attention. Further, solar cells, radiation conditions on- site, a various of PV system components and the prices of electricity are among the aspects to be presented. Chapter 3 shows the methodology used to process datasets and analyse information in this thesis, and the results which these approaches have led to, including presentation of the most suitable PV system to use on the warehouse roof, design of the respective system as well as analysis of the economic impact of the system. Chapter 4 intends to compare the results gained in this thesis with their respective theoretical aspects through discussions. In chapter 5, a summary of the thesis is described as well as conclusion based on former results and discussions. To end with, chapter 6 presents further work that is likely to improve the approach and results of this thesis.

2 Theoretical Background

2.1 Location

As shown in Figure 2 A, the warehouse described in this study is in Tromsø, Norway and is owned by Coop Norge. Goods are delivered to Tromsø from Coops main warehouse in Jessheim, Norway, and subsequently unloaded, sorted with electrical forklifts and shipped onto trucks to Coops grocery stores in Northern Norway. To ensure the goods is kept at a constant temperature while sorting, the warehouse has three temperature zones that providing freezing, cooling, and room temperatures with respective temperatures of $-20°C, 4°C$, and $10°C$. The warehouse has an approximate area of $15\,000\ m^2$, where over half is regulated to maintain temperatures from $4°C$ and below. As shown in Figure 2 B, the roof covers all the buildings area and has a flat construction. Due to temperature regulating, charging of forklifts, and lightning, the warehouse has a yearly electricity consumption of 2,9 GWh.
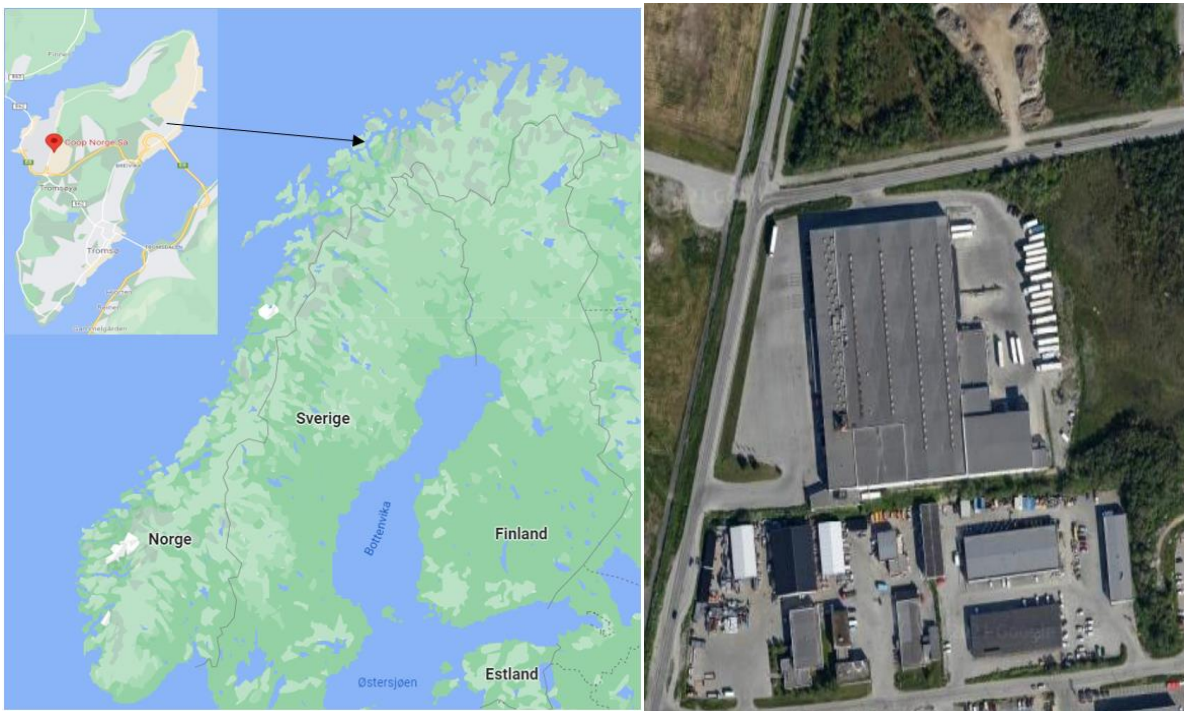
Figure 2 A: Map of Norway, showing the location of Tromsø. The warehouse owned by Coop Norge is located on the west side of the island (Google Maps).

B: Close-up picture of the warehouse investigated in this study. The warehouse is in Tromsø, Norway, and has a roof area of $15\,000\ m^2$, including fans and other objects (Google Maps)

2.2 Solar Cells

2.2.1 The Photovoltaic Effect in Solar Cells

By utilizing radiation made from sunlight, solar photovoltaic cells (solar cells) generate electricity. This process is called "the photovoltaic effect" and is shown in Figure 3 (U.S Energy Information, Administration, 2021). When the energy carrying photons in solar radiation hits a solar cell, some of them are absorbed and contributes to the generation of electricity. The component that absorbs photons inside a solar cell is called a semiconductor. The semiconductors have different properties due to differences in their material doping and are often called n- and p doped. By joining the semiconductors, a p-n junction is made in the area between. Due to energy carrying photons from the sun, normally fixed electrons in the p- doped semiconductors tend to get excited and move to the n- doped semiconductor, creating an electric field in the junction. Before the excitement, an electron in the p- doped semiconductor is in "the valence band" state, with a low energy level. During the excitement from incoming photons, the electron energy level increases. With sufficient energy level increase, the electron moves through the bandgap and reaches "the conduction band" state, in the n- doped semiconductor. The amount of energy required to excite the electron from the valence band to the conduction band is determined by the bandgap. Electrons in the conduction band are called "free electrons" and can create currents with directions decided by the electrical field in the p-n junction. The current of free electrons can then be utilized in electricity production. (Hanania, Stenhouse, & Donev, 2015)
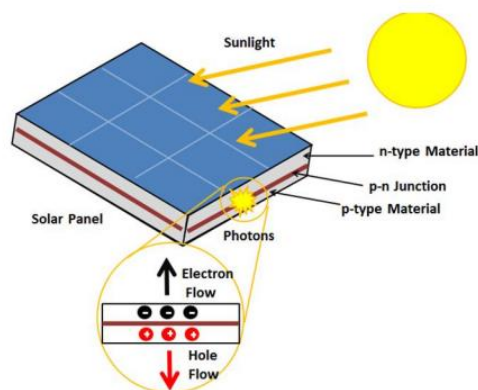
Figure 3: Photovoltaic effect in solar cells created by photons from sunlight. The figure shows the two semiconductors with different properties, and the junction formed between (Energy Education Team, 2015).

2.2.2 Efficiency of the Solar Cell

The efficiency of a solar cell tells how much of the incoming energy from a photon that is generated to electricity. To determine this efficiency, the solar cell is tested by the manufacturer under standard test conditions (STC). To fulfil these conditions, the cell must be tested with an irradiance of $1000 \, W/m^2$ and a cell temperature of $25 \, °C$. Both irradiance and cell temperature tends to deviate from STC values, leading to a different efficiency than stated by the manufacturer (Chandrasiri & Attygalle, 2017).

The efficiency of a solar cell is reduced with temperature due to changes in bandgap characteristics. To excite an electron to a higher energy state in order to make electricity, a particular amount of energy is required. The required energy is related to the bandgap energy of the solar cell, as mentioned in section 2.2.1. Absorbed photons with energy levels exceeding the bandgap energy will only contribute to increasing the cell temperature, rather than electricity production. Unfortunately, increasing the cell temperature leads to a decrease in the bandgap energy. This creates an efficiency drop, where a higher number of photons will have energy levels exceeding the bandgap energy level, contributing to heating and decreases the bandgap further. (Afework, YYelland, & Donev, 2018) This correlation is shown in Equation (1), where the efficiency of a solar cell is given as n_c. Here $n_{ref}, \beta_{ref}, T_c,$ and T_{ref} respectively gives the reference efficiency, the temperature coefficient, the cell temperature, and the reference temperature. From Equation (1) it is proved that a decrease in the cell temperature Tc will make the efficiency rise. This is likely to occur in Tromsø, due to ambient temperatures below the STC value for most of the year (Chandrasiri & Attygalle, 2017).

$$n_c = n_{ref}[1 - \beta_{ref}(T_c - T_{ref})] \tag{1}$$

2.2.3 The Solar Cell as an Electrical Component

As an electrical component, an unilluminated solar cell has similarities with a diode, as it requires sufficient voltage to lead current, and only allows the passing currents to move in a positive direction. When exposed to illumination, the solar cell could be represented by the equivalent called the "one- diode model", shown in Figure 4. In this equivalent, a photoelectric current is provided by a current source (I_{ph}), with a diode and a shunt resistance (R_{sh}) in parallel. The shunt resistance represents the voltage drop occurring due to leakage of charges when moving from the semiconductor to the contacts. The resistance due to components is

7

represented by the series resistance (R_S). The load voltage and load current (V) and (I) is determined by the size of both the current source and the resistances. To utilize the most of power of an illuminated solar cell, it is preferred to have a large shunt resistance and a small series resistance (Nordahl, 2012).
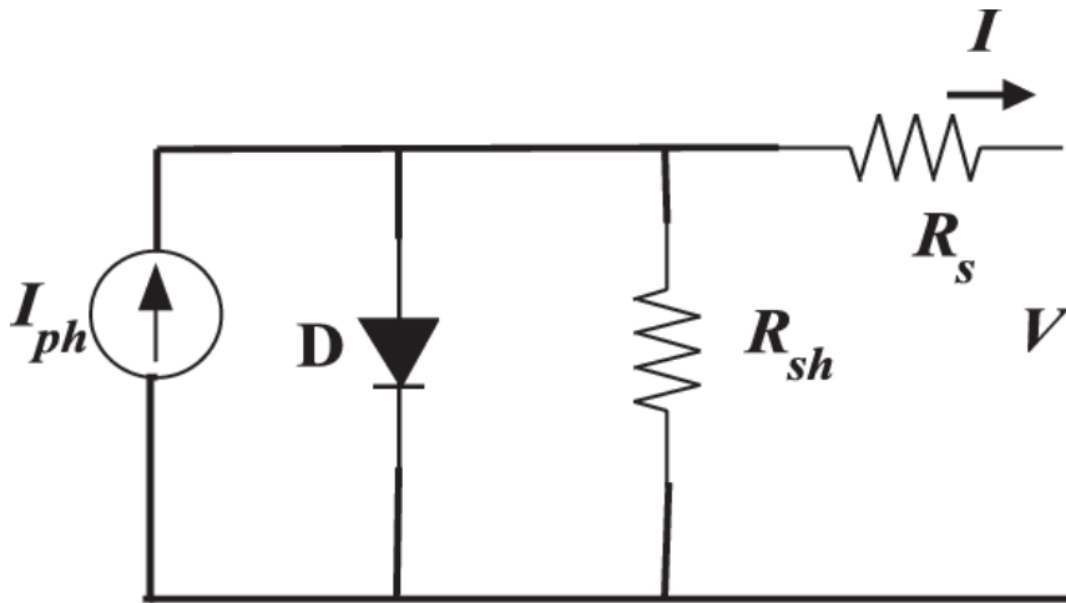
Figure 4: One- diode model representing the equivalent of a solar cell exposed to illumination. The load voltage and load current V and I is determined by the size of the current source and the resistances, respectively represented by I_{ph}, R_{sh}, and R_s. (Tayyan, 2015)

When the current through a solar cell is zero, the circuit in Figure 4 is considered open. In this situation, the highest voltage one can obtain over a solar cell occur, called the open circuit voltage (V_{oc}). As this voltage is inversely proportional with temperature, it is partially settled by the ambient temperature of the solar cell. When the voltage across a solar cell is zero, the cell is considered short circuited. In this situation, the highest possible circuit one can obtain in a solar cell occurs, called the short circuit current (I_{sc}). Optical properties of the solar cell such as reflection and absorption affect the short circuit current, in addition to the cell area and the power of the incoming solar radiation (Honsberg & Bowden, Short- circuit current , 2022).

A solar cell has a point where its reaches maximum efficiency and following produces the highest amount of power. This point is called the Maximum Power Point (MPP) and is continuously affected by the ambient weather conditions such as temperature and irradiation. To ensure maximum production it is desired to combine the output voltage and current in a such

way that MPP is always achieved, as presented in Figure 5. The MPP occurs when the current is located at I_{MP}, and the voltage is located at V_{MP}, and to achieve such conditions, maximum power point tracking (MPPT) is used. MPPT uses algorithms to utilize the best combination of current and voltage for reaching MPP (Faranda & Leva, 2008).
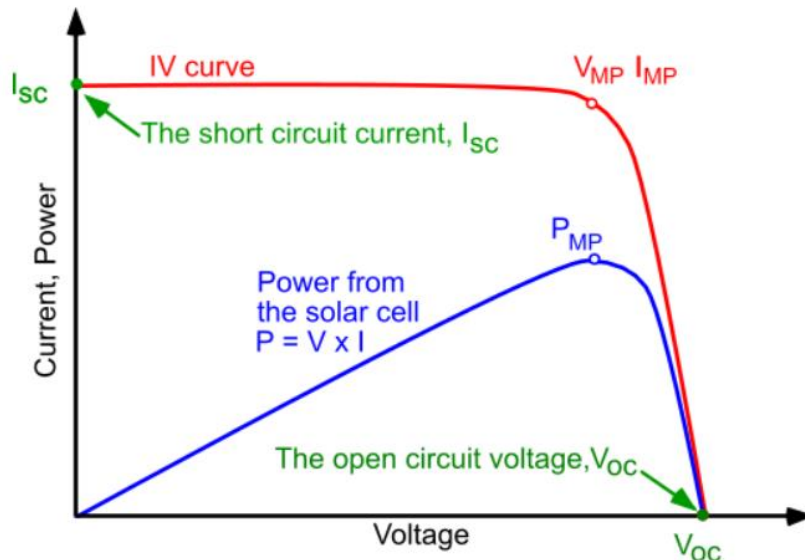
Figure 5: Current- voltage (IV) curve (red) and power- voltage (PV) curve (blue) for a solar cell. I_{sc} and V_{oc} respectively represents the short circuit current and the open circuit voltage for the cell. V_{mp} and I_{mp} respectively gives the ideal voltage and current to be combined for reaching maximum power point (MPP). P_{mp} represents the maximum power output for the PV cell (Honsberg & Bowden, IV Curve, 2022).

2.3 Modules and Strings

A single solar cell produces a voltage of about 0,5 V at the MPP. As higher voltages are more suited for power transport in cables, it is desirable to increase the voltage to higher levels. Kirchhoff's voltage law claims that the sum of voltages in a closed circuit must be zero. Using this as a base, solar cells are connected in series to increase the output voltage. Solar cells in such setups are called a module and are manufactured in many versions. A 400 W module commonly consist of 104 cells, able to provide MPP voltages of 50- 70 V. In addition to increasing the voltage to higher levels, a module offers mechanical protection for the solar cells inside. As solar cells and the electrical connections between them are sensitive to moisture, dust and mechanical damage, the module encapsule makes the fragile components able to operate without being damaged by the surroundings. A cross section of a module is shown in Figure 6, and contains of toughened glass on the top, that gives mechanical protection for the solar cells, followed by an anti- reflective coating ensure to minimise reflection loss. Front and back

electrical contacts are used for current transport. The module core contains of N- type and P-type silicon semiconductors with a junction between them, followed by a back sheet.
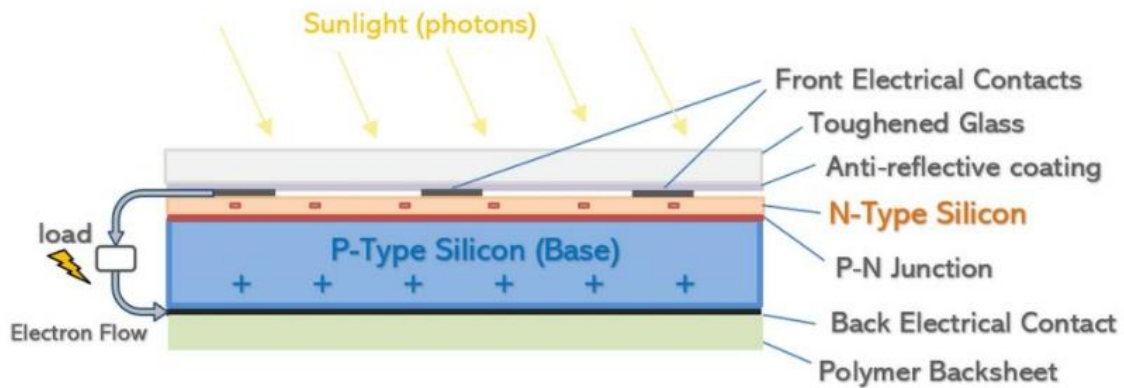
Figure 6: Cross section of a module, presenting the containing layers used for both electricity generation and mechanical protection (Svarc, 2020).

By connecting modules in series, a string is formed. The voltage across a string is the sum of all the individual module voltages whereas the current in such a setup will be equal throughout the circuit and limited to the module providing the lowest amount. This creates limitations for all modules in a string in cases of shadowing. (Åsheim, 2017) (Honsberg & Bowden, Module Structure, 2020)

2.4 String Calculation

To determine the maximum string size, the highest open circuit voltage ($V_{OC,max}$) from the module must be derived. The V_{oc} provided from the manufacturer is measured with standard test conditions, but as this value is inversely proportional with the temperature, the actual V_{oc} in low temperatures may exceed the manufacturer's estimates. This deviation must be considered when designing a PV system in Tromsø, as the locations low ambient temperatures can create voltage peaks causing damage to system components. In addition, voltages exceeding the inverter input voltage range will be cut off, leading to production losses. To protect system components and ensure maximal power production during the voltage peaks caused by the V_{oc} increase in low temperatures, $V_{OC,max}$ is calculated with Equation (2) Here, V_{oc}, Tk_{Voc}, and

T_{STC} respectively represents the open circuit voltage, the open circuit voltage temperature coefficient, and the standard test condition temperature, all provided by the module manufacturer. T_{min} represents the minimum ambient temperature expected for the location. (Honsberg & Bowden, Open- circuit voltage , 2022) .

$$V_{OC,max} = V_{OC} \left(1 + \frac{(T_{min} - T_{STC})\, Tk_{Voc}}{100} \right) \qquad (2)$$

To acquire the maximum open circuit voltage for a module, the maximum string size ($n_{string,max}$) is derived using Equation (3) Here, $V_{inverter,max}$ is the inverter maximum input voltage, and V_{OCmax} is the maximum open circuit voltage for a module, derived by Equation (2). The maximum number of modules in a string is set to avoid exceeding voltage levels for the system components, as this could cause both production losses and damage.

$$n_{string,max} = \frac{V_{inverter,max}}{V_{OC,max}} \qquad (3)$$

To determine the minimum string size, the lowest maximum power point voltage ($V_{MPP,min}$) is derived with Equation (4). Here, V_{MP}, Tk_{Voc}, and T_{STC} respectively represents the maximum power point voltage, the maximum power point temperature coefficient, and the standard test condition temperature, all provided by the module manufacturer. T_{max} represent the maximum ambient temperature for the location, and T_{add} represent the adjustment of temperature due to the installation method.

$$V_{MPP,min} = V_{MPP} \left(1 + \frac{(T_{max} + T_{add} - T_{STC})\, Tk_{Vmp}}{100} \right) \qquad (4)$$

To acquire the lowest MPP voltage for a module, the minimum string size ($n_{string,min}$) is derived using Equation (5). Here, $V_{inverter,min}$ is the inverter minimum input voltage and V_{MPPmin} is the lowest MPP voltage for a module, derived in Equation (4). Approach for the calculations is collected from (Mayfield Renewables , 2018).

$$n_{string,min} = \frac{V_{inverter,min}}{V_{MPPmin}} \qquad (5)$$

2.5 Degradation and Lifetime of Modules

During the years, the module power output is reduced as the modules experience degradation. The level of module degradation variates with location, as it is accelerated by environmental factors such as thermal stress and moisture. Modules in Tromsø are likely to be positively affected by the low temperatures of the location, resulting in a decreased degradation rate. To give accurate predictions for power production during the lifetime of a PV system, degradation of modules must be included. Module manufacturers typically offers both product- and power production warranties of 20- 25 years, ensuring a power production of typically 80- 90% of the power produced in year 1, leading to an annual degradation rate of 0,3- 0,8%. A module continues to produce electricity despite both expired warranties and degradation. The lifetime of a module therefore depends on the decided level for acceptable energy production. (Mow, 2018) (Honsberg & Bowden, Degradation and Failure Modes, 2022)

2.6 Solar Radiation in Tromsø

Solar radiation hitting a surface at the earth occur in the forms of direct and diffuse radiation. Solar radiation that is exposed to scattering before hitting the earth's surface, is called diffuse radiation.

This scattering may originate from dust, clouds, or other particles that can refract the light beams radiated from the sun. The part of the radiation that directly hits the surface without refractions are called direct solar radiation. This type of radiation is highly concentrated with energy and is preferable in terms of energy production by modules. Global radiation contains both diffuse and direct solar radiation and is therefore commonly used to describe the total radiation hitting a surface (Li, Lou, & Lam, 2015).

Solar radiation intensity on a horizontal surface decrease with higher latitudes in the northern hemisphere. In places with high latitudes, solar rays will have a lower angle compared to latitudes near equator, leading to a larger spread for the solar rays, and therefore a lower solar radiation intensity (Climate Science Investigations, 2012). The earth's axis of rotations, shown in Figure 7, has a tilt of 23,5°. For places located in high latitudes, this causes an increase in solar radiation during the summer months, and a decrease in solar radiation during the winter months. Due to the 23,5° tilt in the earth's axis of rotation, Tromsø's high latitude causes

midnight sun from May 18th to July 25th. In this period, solar cells potentially can produce electricity throughout the hole day and night. Tromsø polar nights starts at November 26th and ends on January 17th. During this time, the solar radiation suitable for electricity generation are neglectable, as presented in Figure 8 (Delphin, 2018).
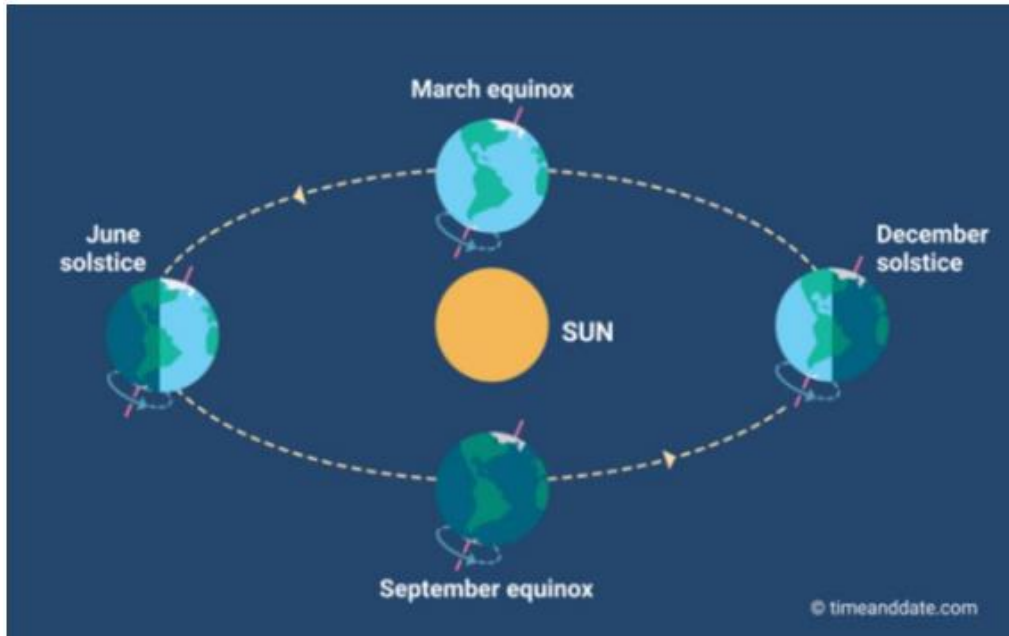
Figure 7: Earth's axis of rotation. For places located in high latitudes, this causes midnights sun during the summer and polar nights during the winter (Hocken, 2021).
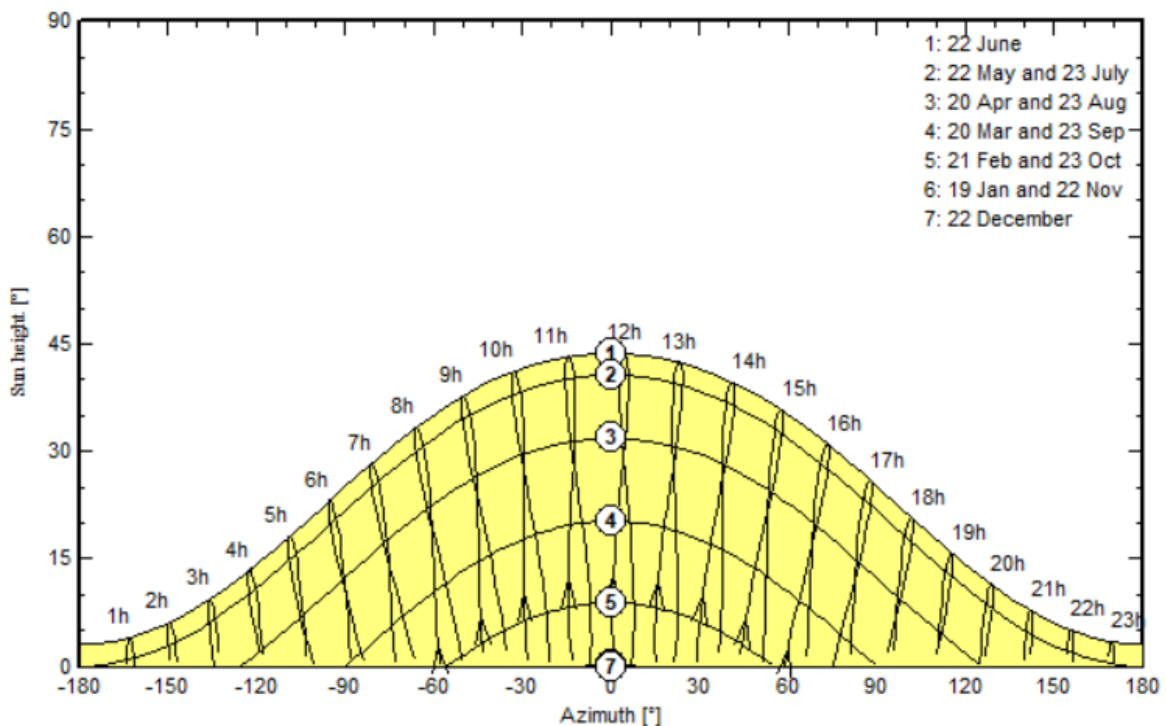
Figure 8: Solar paths for Tromsø during a year, collected from PVsyst.

2.6.1 Solar Radiation on a Tilted, South Orientated Module

The solar radiation intensity on a module is affected by the angle between the module and the solar rays, as the power density of the solar radiation will be at a maximum when the rays are perpendicular to the module surface. Solar radiation on a horizontal module is related to the solar radiation on a corresponding, tilted module with Equation (6). Here, S_{tilted} and $S_{horizontal}$ respectively is the solar radiation intensity on a tilted and a horizontal module. The angle α and θ respectively represents the solar elevation angle and the tilt angle between the module and the horizontal (Honsberg & Bowden, Solar Radiation on a Tilted Surface, 2021).

$$S_{tilted} = \frac{S_{horizontal} * \sin(\alpha + \theta)}{\sin \alpha} \qquad (6)$$

2.6.2 Solar Radiation on a Tilted, East- West Orientated Module

By fixing a module in the northern hemisphere with southwards orientation, the solar radiation potential is usually fully utilized. Giving the module an east- west orientation, the solar radiation strikes with a less ideal angle, resulting in a 15% power decrease compared to south orientated modules. Despite a lower noon peak, east- west orientated modules have higher radiation exposure during morning and afternoon compared to the south orientated modules, as presented in Figure 9 (Rodriguez, 2021).
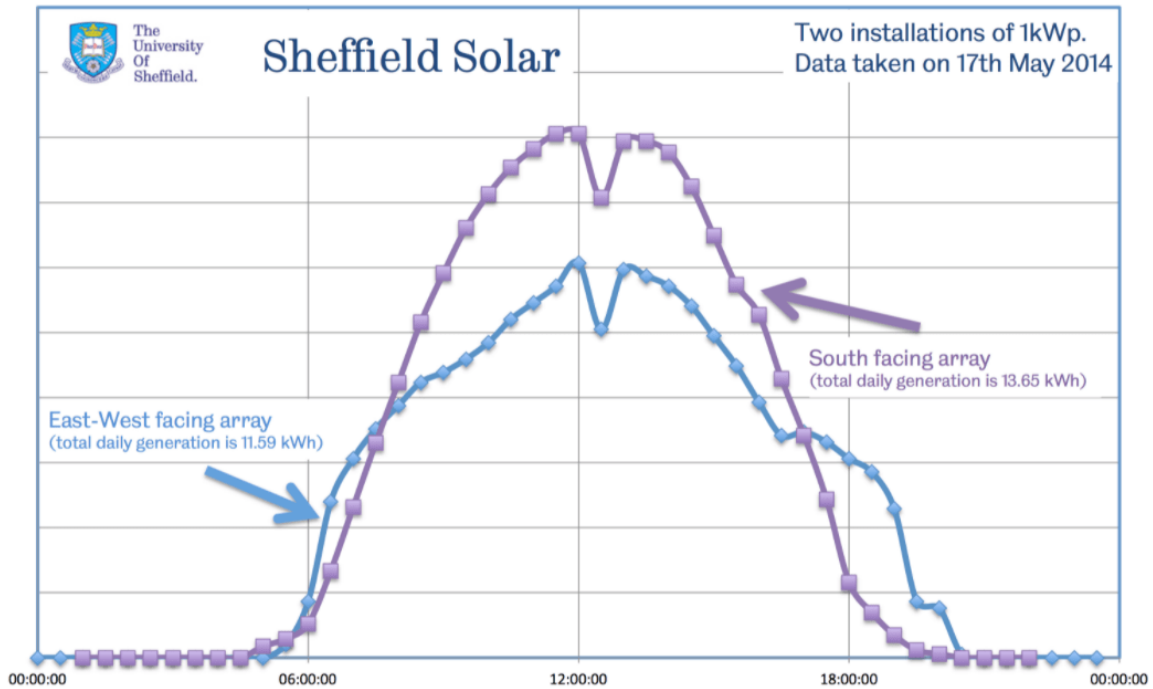
Figure 9: Comparison of energy production from east- west- and south orientated modules. X- axis and y- axis respectively represents time and energy production. Despite a lower midday production, east- west orientated modules offer a higher production in the morning, and afternoon hours, compared to south orientated modules (The University of Sheffield , 2021).

2.7 Ideal Surface Tilt

Due to conditions mentioned in section 2.6.1, a module receives the most energy when obtaining a perpendicular angle with the solar rays. As fixed modules do not have the ability to adjust for the constantly changing solar radiation angle, the mean ideal surface tilt is calculated to utilize most of the radiation during a given part of the year. The ideal tilt for summer months in the northern hemisphere is found with Equation (7) and depends on the geographical latitude (Rensselaer Polytechnic Institute, 2006).

$$\text{Ideal tilt} = (\text{Latitude} * 0{,}9) - 23{,}5° \qquad (7)$$

2.8 Shadowing Between Modules

As shown in Figure 10, shadowing between modules depends on the module height difference, the module row spacing, and the solar elevation angle. Equation (8) calculates the height difference by considering both the module width and the module tilt angle θ. Equation (9) calculates the required module row spacing to avoid shadowing between modules, as shown in Figure 10 , by considering the module height difference and the minimum solar elevation angle α. The row width is calculated with Equation (10), and represents the total space occupied by one tilted module with proper module row spacing to avoid shadowing (Diehl, 2020)
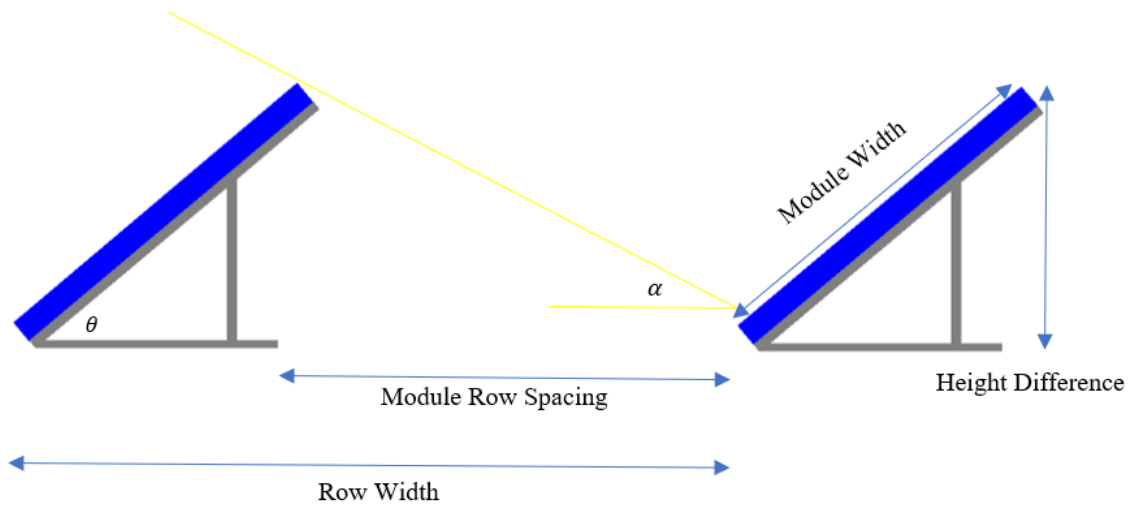
Figure 10: Distances to consider for avoiding shadowing between modules. The solar elevation angle is represented by α, and the module tilt is represented by θ (Diehl, 2020).

$$Height\ Difference = Module\ Width * sin(\theta) \qquad (8)$$

$$Module\ row\ spacing = \frac{Height\ Difference}{tan(\alpha)} \qquad (9)$$

$$Row\ width = Module\ row\ spacing + [cos(\theta) * Module\ Width] \qquad (10)$$

2.9 The PV System

2.9.1 The Inverter

For the grid tied system investigated in this study, the inverter transforms the incoming DC power from the modules into outgoing AC power with frequencies usable for supplying the grid. Additionally, the inverter ensures optimal power output by maximum power point tracking (MPPT) (Chiesa, Simpson, & Stefancich, 2016). Among the several types of inverters, this study focusses on the central inverter and the three-phase multi string inverter. The central inverter can handle high amounts of power and is therefore frequently used in large utility scale plants. Due to the large capacity, only a few central inverters are needed in a PV system, leading to a lower cost compared to other inverters. Despite the high capacity of a central inverter, the string voltage in these systems usually do not exceed 1000 V due to limitations within the electrical components. Therefore, to fully utilize the capacity of the central inverter, strings are connected in parallel by using string combiners. This type of connection increases the current, and the power in the circuit, without exceeding the maximum system voltage. Such setup entails limitations for the central inverters in terms of energy optimization, as they normally have one or a few MPPTs to optimize the power production from many modules.

The multi string inverter handles a lower amount of power compared to the central inverter, and a higher number is needed to cover the same amount of power. In situations when several inverters are used, proper communication systems must be used to ensure sufficient energy production for the PV system. Multi string inverters are suited with multiple string inputs, and often several MPPTs. Due to a relatively low number of modules per MPPT, such inverter offers high energy optimization from PV system as fewer modules are affected in cases of shadowing. Generally, central inverters are recommended to use in PV system with a power of over 10 MW and string inverters are recommenced for 1-10 MW (Misbrener, 2018).

The inverter loading ratio (ILR) describes the relation between the peak DC power from the modules and the nominal AC power from the inverter. PV systems are commonly designed to have undersized inverters, leading to a ILR greater than 1. This is preferred since modules produce below its nominal power most of the hours during a day. During these times, an undersized inverter will harvest a greater amount of energy, as it has the highest efficiency during moderate to high levels of energy production. Despite being beneficial in times of low

17

power production, an undersized inverter does not have the capacity to fully process all the module provided DC power in times of high production. This causes loss of energy that exceeds the maximum capacity of the inverter and is called inverter clipping. Despite the inverter clipping, the ILR is often calculated to be in between 1,13- 1,30 for individual systems, as this is found to be most beneficial (Bromberg, 2021). As mentioned, losses occur in the process of transforming DC power into AC power. The size of the losses depends on the inverter efficiency, and the inverter efficiency variates with the input power provided from the modules. In cases with moderate to high levels of energy production the efficiency of the inverter maintains 90 –98%, as shown in Figure 11. (Pearsall, 2017)

Among characteristics to consider is the inverter input voltage range. If a string provides voltages outside this range, the produced power at the given time is not fully utilized as the inverter only transforms incoming DC power within certain voltages. It is desirable to pair the string and inverter in a such way that the string voltage is within the input voltage range inn all time of significant production (Åsheim, 2017).
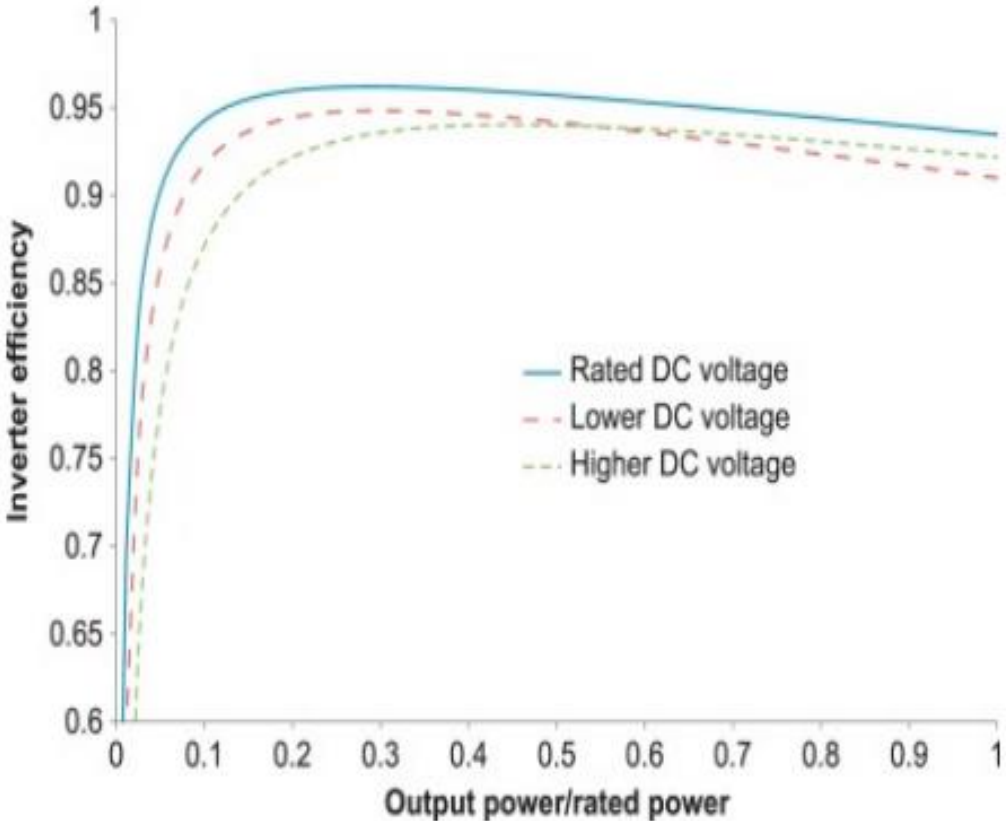
Figure 11: Inverter efficiency plotted as a function of the DC input voltage. The efficiency peak when the rated DC input voltage is provided. Lower and higher DC input voltage will lead to a decrease in efficiency. (Pearsall, 2017)

2.9.2 Conductors

The current carrying capacity (CCC) for a conductor is the maximal amperage possible to obtain without surpassing the thermal limit of either the conductor or the conductor insulation, as this leads to degeneration of the isolation and a reduction of lifetime. To avoid such damage, factors affecting the conductor temperature such as the Joule Effect, environmental heat exchange, and distance between the conductors are considered during cable sizing. The Joule effect increases the conductor temperature and thereby reduces the CCC due to thermal energy generation occurring as a current is carried. Environmental heat exchange also affects the conductor temperature and is caused by solar radiation and the ambient temperature. Normally, an ambient temperature of $30°C$ is used as a reference value when determining a conductor's CCC, for ambient temperatures exceeding the reference value a correction factor must be used. A similar factor must be added if parallel conductors are installed in a such way that they touch, as the occurring heat exchange leads to decreased CCC for each conductor involved. If correction factors from either the Joule Effect, environmental heat exchange, or the distance between the conductors causes the chosen conductor to have insufficient CCC, a large cross section must be used. The type of conductor and conductor isolation needs to be considered, as the materials have differences in their conductivity and thermal properties (Dupin & Michiorri, 2017) (Electrical Installation by Schneider Electric , 2021).

To determine the minimum cross section area A for a cable to avoid surpassing the limit for allowed voltage drop, Equation (11) is used. Here, I_{Load} is the current carried through the cable, L_{cable} is the route length of the cable, multiplied by a factor b to represent the total length. The resistivity of the conductor is represented by ρ, V is the system voltage and ΔV is the percentage voltage drop in the cable.

$$A = \frac{I_{cable} * b * L_{cable} * \rho}{V * \Delta V} \tag{11}$$

2.9.3 Performance Ratio

Performance ratio gives the quality of a PV system by comparing the theoretical and the actual energy output for the system. Ideally, this value should be 100%, but due to losses it is considerably lower. Factors that affect the performance ratio could be shading of the module, dissipation of solar radiation, the temperature of the module, conduction losses from cables, and the efficiency factor of power electronics, such as the inverter. High performance PV

systems can have a performance ratio surpassing 90%. To find the performance ratio, the actual energy output from a system is divided by the theoretical energy output for the same system. In cases when the actual energy output is not available, a performance ratio could be assumed by analysing the affecting factors mentioned (SMA Solar, 2020).

2.9.4 Energy Production from a PV System

The energy production from a PV system depends on the total area covered exclusively by modules, the module efficiency, the average incoming solar radiation on the given surface, and the performance ratio that considers the loss in the various components of the PV system. Equation (12) calculates the energy output for a PV system. Here, A is the total area, r is the module efficiency, H is the incoming solar radiation on given surface, and PR is the performance ratio (Carl, 2014).

$$E = A \cdot r \cdot H \cdot PR \qquad (12)$$

2.9.5 The Weighted Average Cost of Capital for a PV System

The weighted average cost of capital (WACC) is a measure to evaluate the return of invested capital and is a central component in calculating the net present value. The WACC sums up the cost of both debt and equity and covers the effect of inflation. (BEREC, 2017). The WACC for utility- scale PV systems in Europe spans from 2,6- 5,0% (IEA, 2020).

2.10 PVsyst

To simulate a system in PVsyst, the plane orientation for the modules needs to be chosen, where both the azimuth angle and the module tilt needs to be defined. System components such as modules, batteries and inverters also need to be chosen, in addition to deciding the area to use. To make the simulation more accurate, detailed parameters such as wiring, shadings, thermal behaviour, and module quality can be adjusted. PVsyst uses the Meteonorm database to give monthly meteorological data for a given location. Hourly values are also created synthetically, using stochastic models.

Over 8 000 different weather stations all over the world are utilized to provide data to the Meteonorm database. These ground stations provide radiation, temperature, humidity, and wind data. When using PVsyst to simulate the solar radiation on a given place, data from the nearest located ground stations are used. In remote places with no ground station located within a 50 km distance, satellite data is used to provide accurate information. In places located more than 30 km from a ground station, a mixture of data from satellite and ground station data are used. (PVsyst, 2022). There are two ground stations that provides to the Meteonorm database in Tromsø. These stations are in located in Bjorvik and Guleng, with respective distances of 0.2 km and 3.23 km to Coops warehouse, shown in Figure 12. As ground stations located within 50 km from the site are used to collect data, both Bjorvik and Guleng are likely to be used for simulations done in this study. Bjorvik is only 0,2 km from Coops warehouse and is likely to be chosen as nearest ground station by PVsyst.

Figure 12: Meteonorm databases in Tromsø, located in Bjorvik and Guleng with respective distances of 0,2 km and 3,23 km to Coop's warehouse.

2.11 Norwegian Electricity Prices

Due to limitations in transmission capacity, the Norwegian power grid is divided into five price regions as presented in Figure 13. Northern Norway, therein Tromsø, is located within region NO4, characterized as a price region with high power production and low power demand. As most of the region's energy production surplus cannot be transmitted southwards due to limitations of the gird, NO4 has the lowest electricity prices of all price regions. NVE predicts the electricity prices in NO4 to increase in the future, as establishment of new industries, and electrification of the existing, rapidly increases the regions electricity demand. In addition, development of the Swedish power grid is planned, resulting in an increased transmission capacity between NO4 and Scandinavia. Future projected electricity prices between 2025 and 2040 for Northern and Southern Norway are presented in Figure 14 in cases of high, basic, and low CO_2 prices (NVE, 2021).

Figure 13: The five price regions in Norway, made due to limitations in transmission capacity. Tromsø is in price region 4 (NO4) (Statnett, 2022).
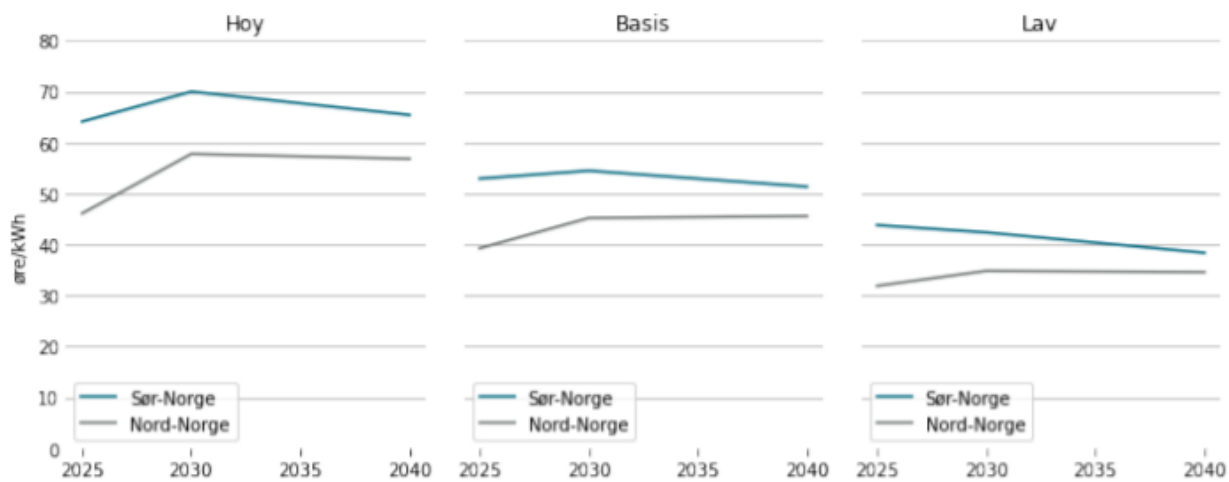
Figure 14: Future electricity prices for Northern- and Southern Norway for high, basic, and low Co2 prices. The price difference increases with time in all cases due growth in both power demand and transmission capacity for Northern Norway (NVE, 2021).

3   Methodology and Results

3.1   Energy Consumption for the Warehouse

Monthly energy consumption data for the warehouse is provided by Coop. The energy consumption is compared with the mean temperature in Tromsø, collected from met.no, to find correlations and gain a deeper understanding of the trends in the warehouse energy consumption. In Figure 15, the blue plot represents the monthly energy consumption for the warehouse during 2020. The consumption reaches its maximum in July, with 278 000 kWh a month, -and its minimum in November, with 220 690 kWh a month, whereas the annual energy consumption is 2 908 227 kWh. The results of Figure 15 show a significantly higher demand for electricity in May, June, July and August. The blue plot represents the mean temperature in Tromsø for each month in 2020. Like the energy consumption, the mean temperature tends to be highest in the summer months, and lower during the remaining year, spanning from -1,8 °C in March, to 13°C in July. The result of Figure 15 gives a correlation between energy consumption and the ambient temperature for most of the months.
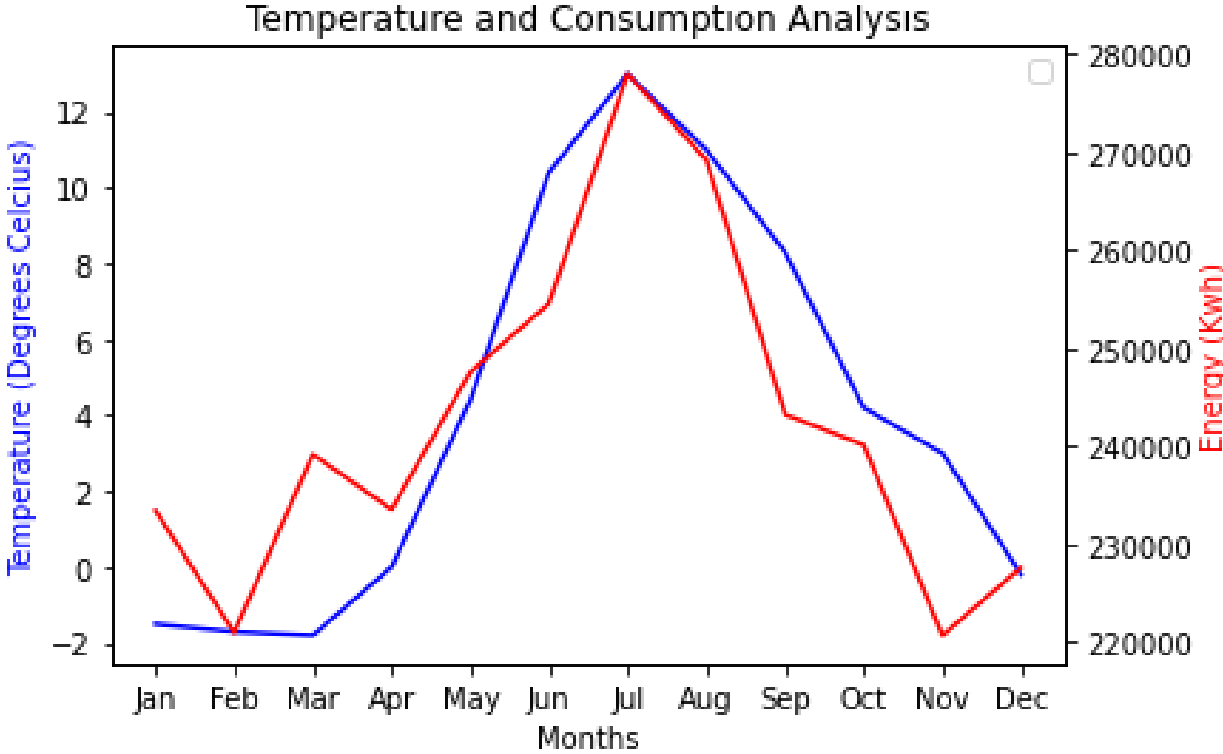
Figure 15: Monthly energy consumption (kWh) for the warehouse and monthly mean temperature (°C) in Tromsø during 2020, respectively represented by red and blue plots. Both the consumption and the temperature peak occur in July, with a monthly consumption of 278 000 kWh and a monthly mean temperature of 13,0°C. A correlation between the plots is found in most months during the year.

25

3.2 Assigned Area for Module Installation

To determine the area to use for module installation, a completely overview of the roof is necessary. For that purpose, ArcGIS and Google Maps are used in combination a visual inspection of the roof. Fans and other objects in conflict with the modules are mapped, and dimensions are collected by using measuring tools in ArcGIS. The area chosen for module installation is shown in Figure 16, forming three identical columns to avoid coverage of fans on the roof. Each column has a length of 130 m and a width of 14 m, resulting in a separate area of 1778 m^2 and a combined area of 5334 m^2 to use for module installations, as presented in Table 1.

Table 1: Dimensions for the assigned roof area to use for module installation.

Column Length	130 m
Column Width	14 m
Column Area	1 820 m^2
Total Area, Three Columns	5 460 m^2

Figure 16: Assigned area for module installation on Coops warehouse roof, consisting of three similar columns with individual dimensions of 14 m 130 m, forming a combined area of 5460 m^2.*

26

3.3 The PV Systems and their Areas

This study investigates three different PV systems to find the most suited for mounting on a warehouse roof in Tromsø. Two of the installations have a tilt with respect to the horizonal plane, and to determine the tilt value of these, Equation (7) is used. It is chosen to prioritize the ideal tilt during summer months, as the solar radiation potential in Tromsø is considerably higher in this period compared to the remaining parts of the year. The systems that are considered in this study are Horizontal Modules (HM), 40° Tilted South orientated Modules (TSM), and 40° Tilted East- West orientated Modules (TEWM).

For all systems it is assumed that 5% of the assigned area is subtracted to ensure proper distances to other modules and objects. For both the systems with tilted modules (HM and TEWM) shadowing of the modules behind is a considerable challenge. To avoid such issue, sufficient inter row distances are ensured by following the approach for module raw spacing calculations, presented in section 2.8. From May to July the electricity production reaches significant values, and the minimum elevation angle is therefore based on the suns position within this time, found by using Figure 8. Table 2 shows the maximum area to fill with modules after inter- row spaces and distances to objects on the roof are considered. The system with TSM utilize least of the available roof area, as its installation requires large distances between modules to avoid shadowing. The triangle- shaped stands used by TEWM proves to be efficient regarding area utilization, giving the respective system the highest utilization. Section 3.3.1, 3.3.2, and 3.3.3 derives the results from Table 2.

Table 2: Area to be filled with modules for three different PV systems after inter- row spaces and distances to objects on the roof are considered. The available roof area is 5460 m^2

System	Total module area (m^2)
Horizontal	5 187
40° tilted, south orientated modules	3 210
40° tilted, east- west orientated modules	6 134

3.3.1 Horizontal Modules

As these modules are mounted directly to the roof, no distances due to shadowing is considered. By taking the total area of $5460\ m^2$ from Table 1 as a stand and subtract 5% due to necessary distances, the modules cover an area of $5\ 187\ m^2$.

3.3.2 Tilted Modules with South Orientation

With the purpose of finding the area to be filled with TSM, the row width is calculated to consider proper distances to reduce shadowing from May to July, as presented in Figure 17. With the purpose of determine the row width, the module height difference HD_m is calculated with Equation (8) to 1,08 m. Equation (9) states that a module with this height difference exposed to a solar elevation angle α of 40°, requires a module row spacing S_{mr} of 1,29 m to avoid shadowing the modules behind. The row width W_r is calculated with Equation (10) to be 2,58 m and represents the width of the module and the occupied space behind it to avoid shadowing nearby modules. Using a row width of 2,58 m, the total module area possible to install on the roof in Figure 16 is found to be $3\ 210\ m^2$. The complete calculation is presented in Appendix C.
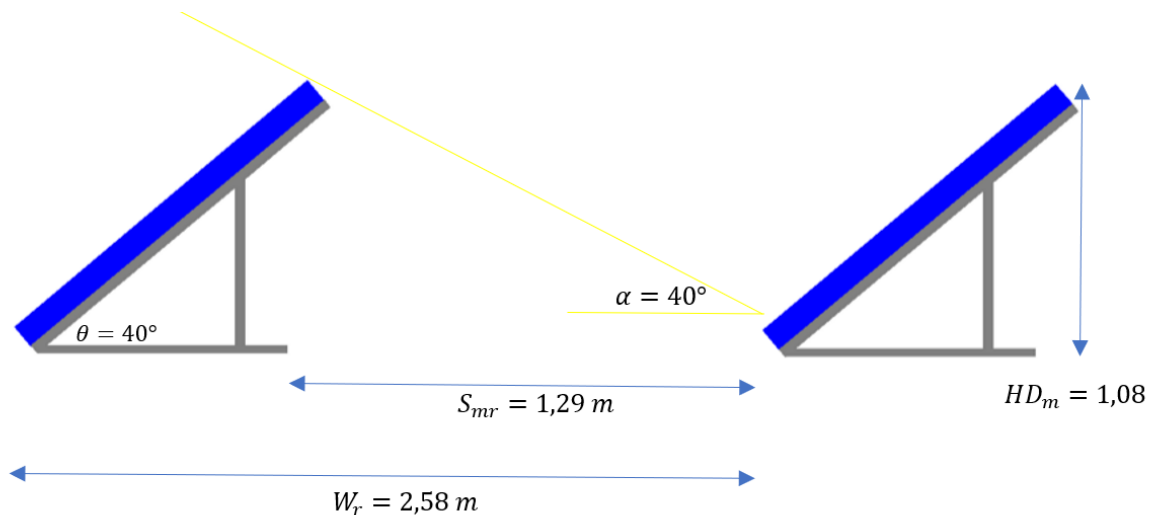
Figure 17: Shadowing calculations for 40° tilted south orientated modules, presenting the module row spacing S_{mr}, the row width W_r, and the module height difference HD_m. The angles θ and α respectively represent the module tilt and the minimum solar elevation angle.

3.3.3 Tilted Modules with East- West Orientation

To find the area to be filled with TEWM, the row width is calculated to consider proper distances due to shadowing, as presented in Figure 18. With the purpose of determine the row width, the module height difference HD_m is calculated with Equation (8) to 0,67 m. This is less than the TSM as the TEWM are mounted with the long side horizontally. Equation (9) shows that a module with this height difference exposed to a solar elevation angle of 40° requires a module row spacing S_{mr} of 0,8 m to avoid shadowing the modules behind.

The row width W_r is calculated with Equation (10) to be 1,6 m and represents the width of the module and the occupied space behind it to avoid shadowing nearby modules. Due to practical reasons, 15 cm is added between each row of modules, increasing the W_r to 1,75 m. The additional W_r results in a minimum solar elevation angle of 35° before shadowing occur. Using the row width of 1,75 m, the total module area possible to install on the roof in Figure 16 is found to be $6134 \; m^2$, including the assumption that 5% of the area is unused due to spacing between modules. The complete calculation is presented in Appendix C
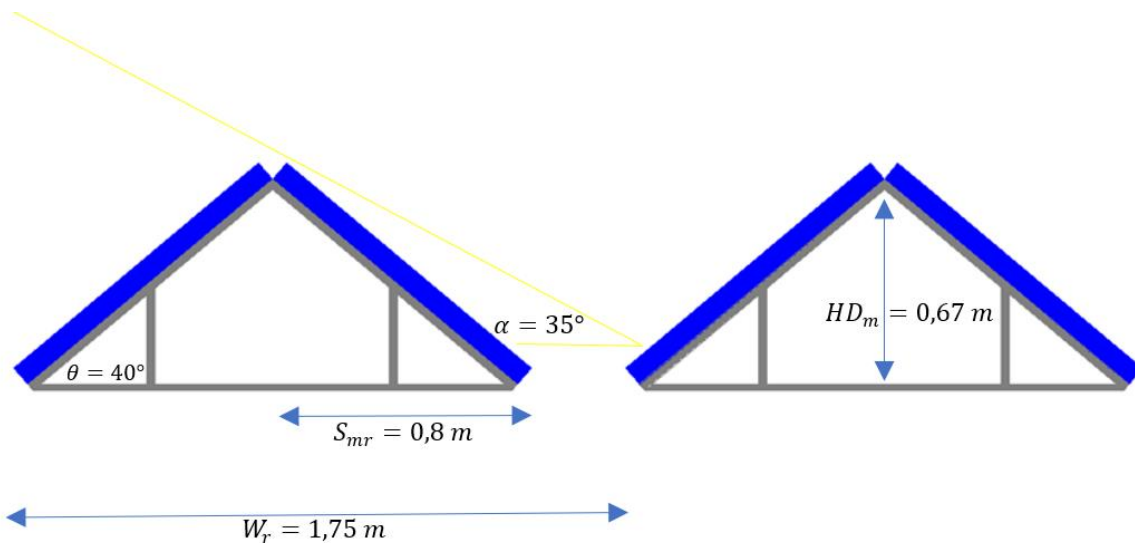
Figure 18: Shadowing calculations for $40°$ tilted east- west orientated modules, presenting the module row spacing S_{mr}, the row width W_r, and the module height difference HD_m. The angles θ and α respectively represent the module tilt and the minimum solar elevation angle.

3.4 Solar Radiation

3.4.1 Solar Radiation from ArcGIS

Deriving solar radiation potential for the warehouse roof, results from both ArcGIS and PVsyst are derived and compared as the comparison of several estimates is desired to ensure the most realistic radiation potential. To determine monthly solar radiation for a horizontal module on the warehouse roof, Area Solar Radiation (ASR) in ArcGIS is used. This tool derives the solar radiation of a given area in regard of latitude, solar position and solar declination, in units of kilo watt hours per square meter (kWh/m^2). For this study, the given area contains the warehouse roof. ASR allows different time configurations, and for this study, monthly calculations were done by iterating through each month of a year. Direct and diffuse radiation conditions, mentioned in section 2.6, are considered and is decided by the diffuse proportion. This proportion gives the part of global radiation that is diffuse, and spans from 0 to 1. For calculations done in this study the diffuse proportion is set to 0,3, which represents generally clear sky conditions (ArcGIS Pro, 2021). To determine monthly solar radiation (kWh/m^2) on TSM, derived values for radiation on a HM were used with Equation (6), as this represents the correlation between the two types of radiation. To calculate the solar radiation (kWh/m^2) on TEWM, a loss factor of 20% is implemented to the already derived values for monthly radiation on a tilted, south orientated plane. Figure 19 shows the solar radiation potential on the warehouse roof for the systems mentioned in section 3.3, while Table 3 shows the radiation potential in detail. The TSM have the highest yearly radiation with $952\ kWh/m^2$, whereas the TEWM have a yearly radiation of $733\ kWh/m^2$, followed by the HM with a yearly radiation of $597,7\ kWh/m^2$.
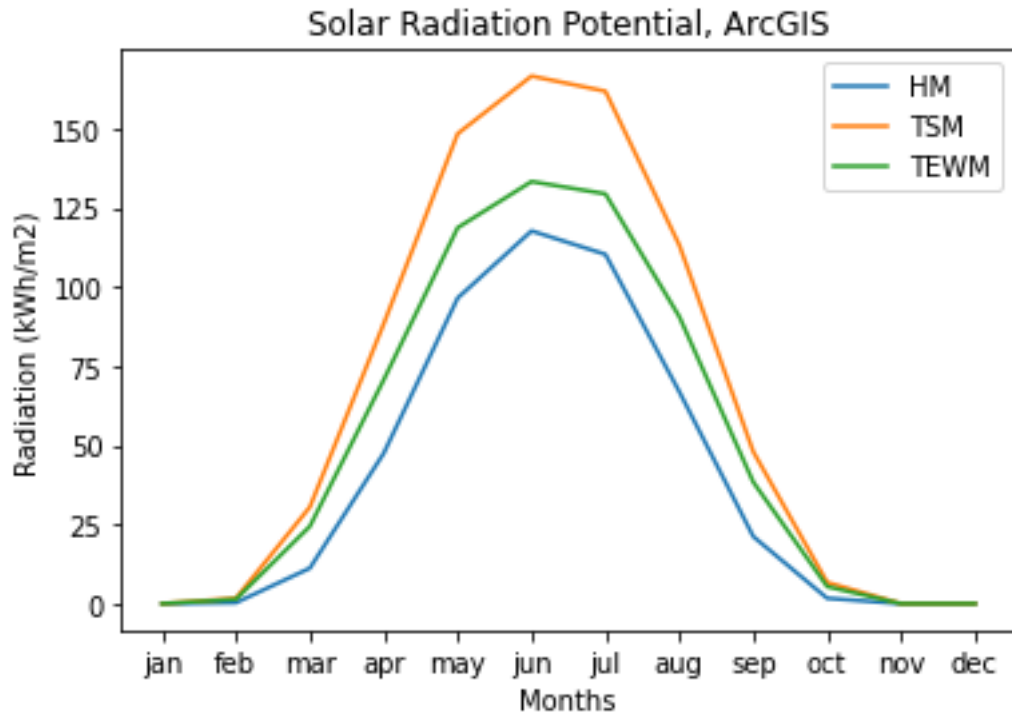
Figure 19: ArcGIS monthly solar radiation potential for the horizontal, $40°$ tilted south orientated, and $40°$ tilted east-west orientated modules. The x- axis gives months for one year, and the y- axis gives the solar radiation potential in (kWh/m^2). South orientated modules gain highest radiation potential, followed by the east- west orientated modules, whereas the horizontal modules get the least radiation per square meter.

Table 3: Monthly solar radiation potential from ArcGIS in kWh/m^2 for horizontal modules (HM), $40°$ tilted south orientated modules (TSM), and $40°$ tilted east west orientated modules (TEWM)

Month	HM	TSM	TEWM
January	0	0	0
February	0,3	1,7	1,3
March	11,2	30,5	23,5
April	47,5	88,4	68,1
May	96,5	148,4	118,7
June	117,7	166,6	128,3
July	110,3	161,8	124,6
August	66,9	113,2	87,2
September	21,2	48,0	37,0
October	1,7	6,7	5,2
November	0	0	0
December	0	0	0
Total	473,3	765,3	612,2

3.4.2 Solar Radiation from PVsyst

To estimate the solar radiation potential for the three systems mentioned in section 3.3, three separate simulations are done in PVsyst. The system component types such as modules and inverters are equal for the three simulations, whereas the number of components varies as the three systems have different area utilization to avoid shadowing. The plots are used with the purpose of comparing PVsyst values with results extracted from ArcGIS, to look for correlations.

For this study, the location is selected to be Coop's warehouse in Tromsø. Here, there are two ground stations included in the Meteonorm database, located in Bjorvik and Guleng. During simulations, solar radiation data from these stations will be utilized as a basis (PVsyst, 2022). Figure 19 shows the solar radiation potential in kWh/m^2 on the warehouse roof for the systems mentioned in section 3.3, while

Table 3 shows the radiation potential in detail. TSM have the highest yearly radiation with $952\ kWh/m^2$, followed by TEWM with a yearly radiation of $733\ kWh/m^2$. HM receives a yearly radiation of $597{,}7\ kWh/m^2$, as a result of the least ideal angle of all systems.
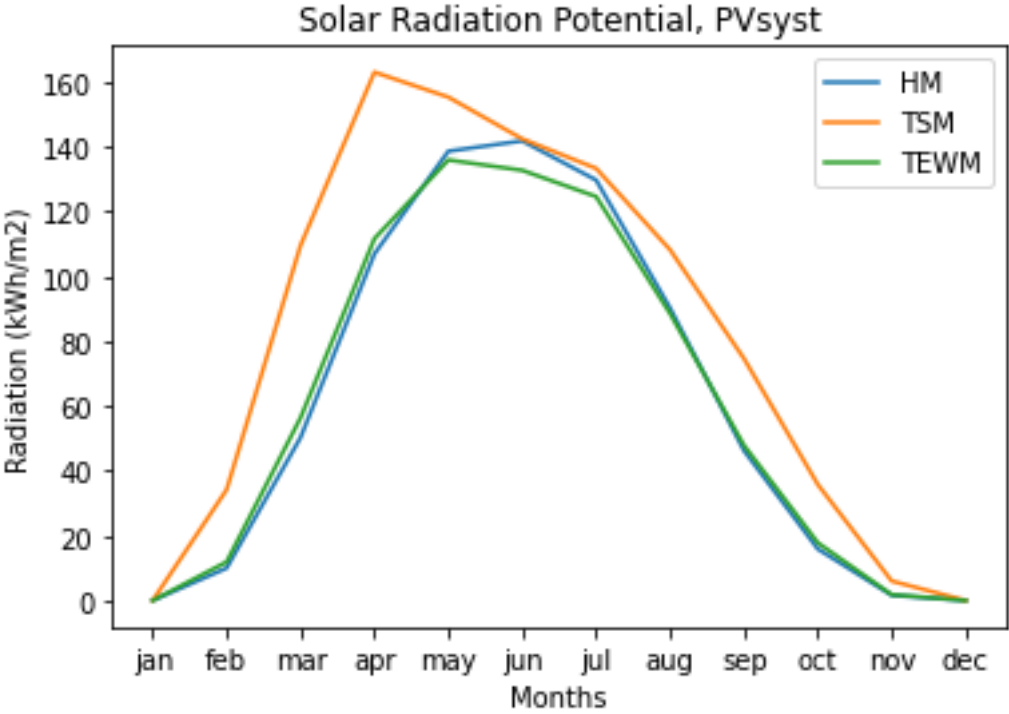
Figure 20: PVsyst monthly solar radiation potential for horizontal modules (HM), $40°$ tilted with south orientated modules (TSM), and $40°$ tilted east- west orientated modules (TEWM). The x- axis gives months for one year, and the y- axis gives the solar radiation potential in (kWh/m^2). TSM gain the highest radiation potential, followed by the HM, whereas the TEWM gets the least radiation per square meter.

Table 4: Monthly solar radiation potential from PVsyst in kWh/m^2 for horizontal modules (HM), 40° tilted south orientated modules (TSM), and 40° tilted east west orientated modules (TEWM).

Month	HM	TSM	TEWM
January	0	0	0
February	10	34,2	11,9
March	50,3	109,6	56,4
April	107,0	163,1	111,7
May	138,7	155,4	136,0
June	141,9	142,5	132,8
July	129,8	133,4	124,7
August	90,3	108,3	88,6
September	46,3	74,7	47,9
October	15,9	35,8	17,8
November	1,6	6,0	1,8
December	0	0	0
Total	731,8	963	729,6

3.4.3 Comparison of Solar Radiation from ArcGIS and PVsyst

To simulate the solar radiation potential for the warehouse roof, both PVsyst and ArcGIS used. Figure 21, Figure 22, and Figure 23 respectively presents the comparison of these estimates for HM, TSM and TEWM. For the respective systems, PVsyst to estimate 35%, 21% and 15% higher values for annual radiation compared to ArcGIS. For the HM, ArcGIS values never exceed the results from PVsyst, although the difference between the results decreases from July and out the year. For the TSM, PVsyst values peaks in April, and although ArcGIS has a similar peak value this does not occur until June. For TWEM, PVsyst values are higher until July. From July and throughout the year, the radiation values from the two simulations are similar.
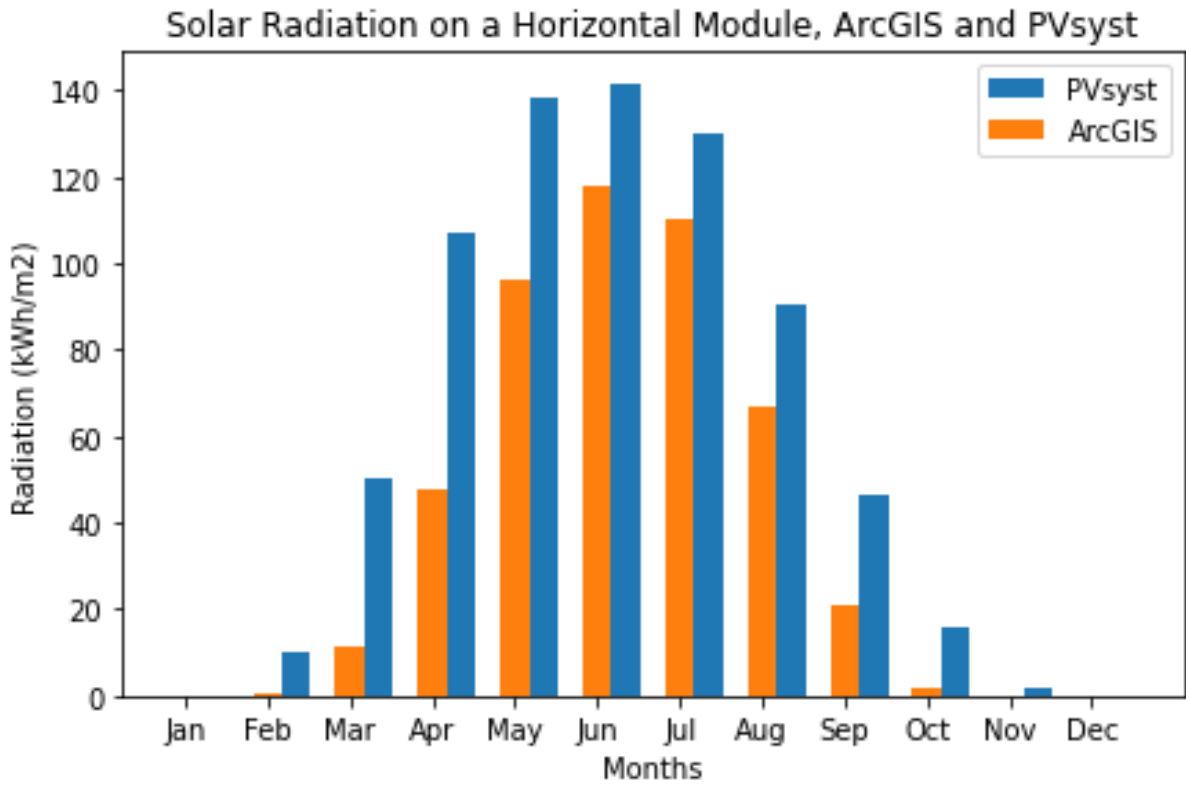
Figure 21: Monthly horizontal radiation potential (kWh/m^2) on a horizontal module compared for PVsyst and ArcGIS.
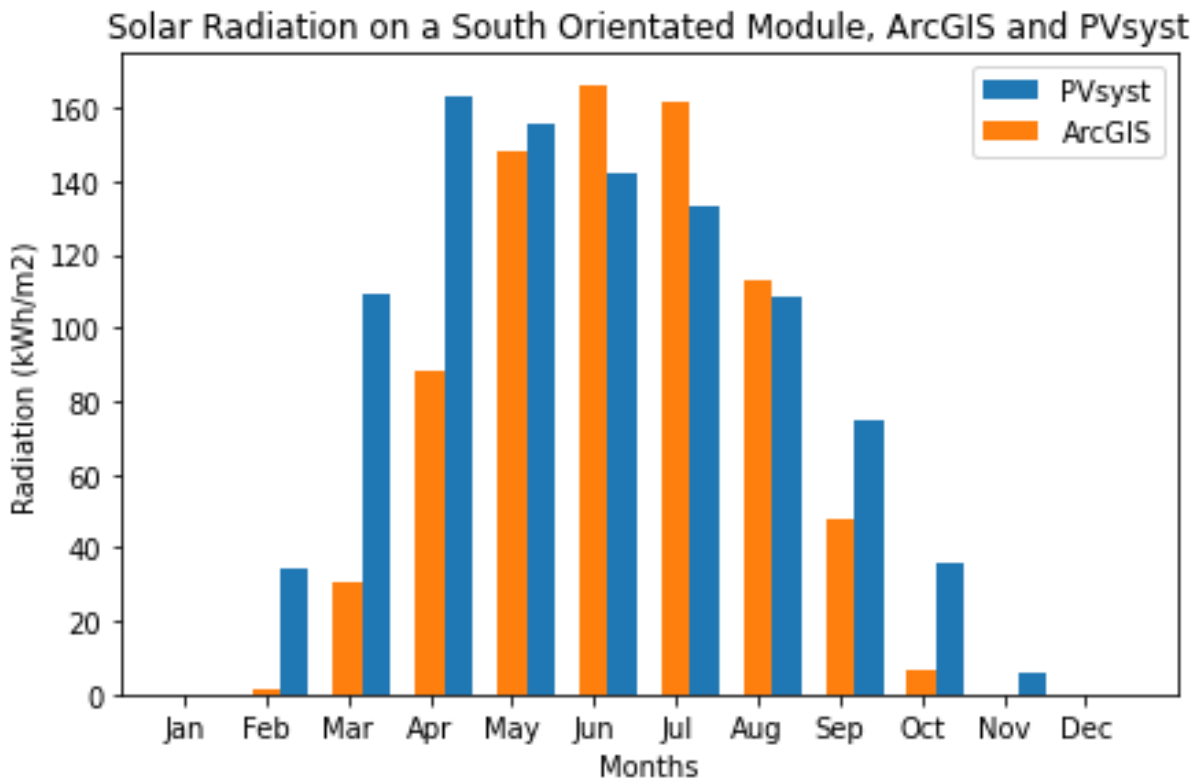
Figure 22. Monthly radiation potential (kWh/m^2) on a 40° tilted, south orientated module compared for PVsyst and ArcGIS.
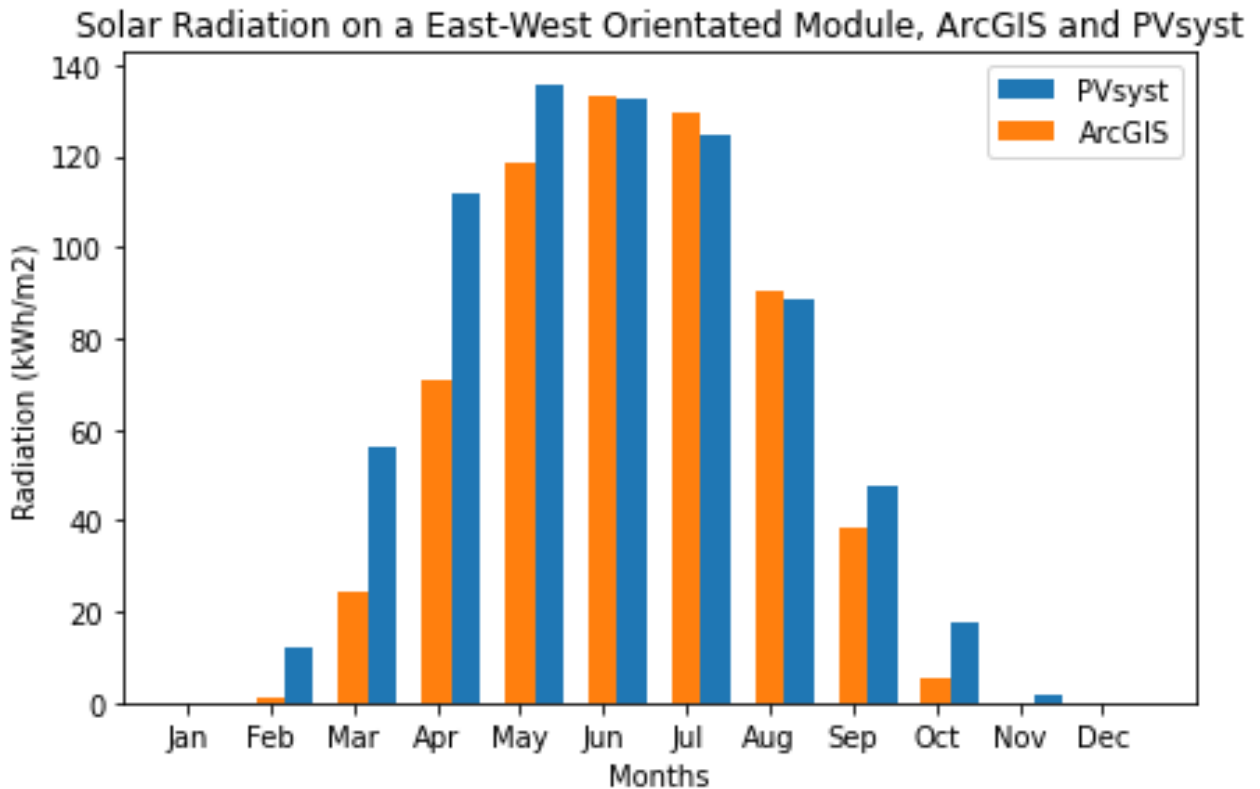
Figure 23. Monthly radiation potential (kWh/m^2) on a 40° tilted, east west orientated module compared for PVsyst and ArcGIS.

3.5 Energy Production

To derive energy production for the three systems presented in 3.3, Equation (12) is used. Solar radiation values in the following calculations are collected from ArcGIS and presented in Table 3, whereas available roof areas are collected from Table 2. The module efficiency is 22,5% based information from the module chosen in section 3.7, and the performance ratio is derived to 85% by comparing theoretical values mentioned in section 2.9.3 with the physical conditions for the given location in this study. The probability of shading from surrounding objects is considered low, as the warehouse is located far from high objects such as threes and buildings. Shading from snow also is considered low due to strong winds. Conduction losses in cables are assumed to be small, as the low mean temperature improves the conductivity, mentioned in section 2.8. It is assumed that the following physical conditions contributes to a higher performance ratio. Figure 24 presents the monthly energy production for the three systems, where the respectively annual production for HM, TSM and TEWM are 469,2 MWh, 469,8 MWh and 718,2 MWh.

HM and TSM produces similar amounts of power during the year. As the tilted modules give higher utilization during low solar elevation angles, TSM produce the most during spring and fall. During May, June, and July, HM produces the most as the solar elevation angle reaches sufficient levels for such modules to harvest energy.
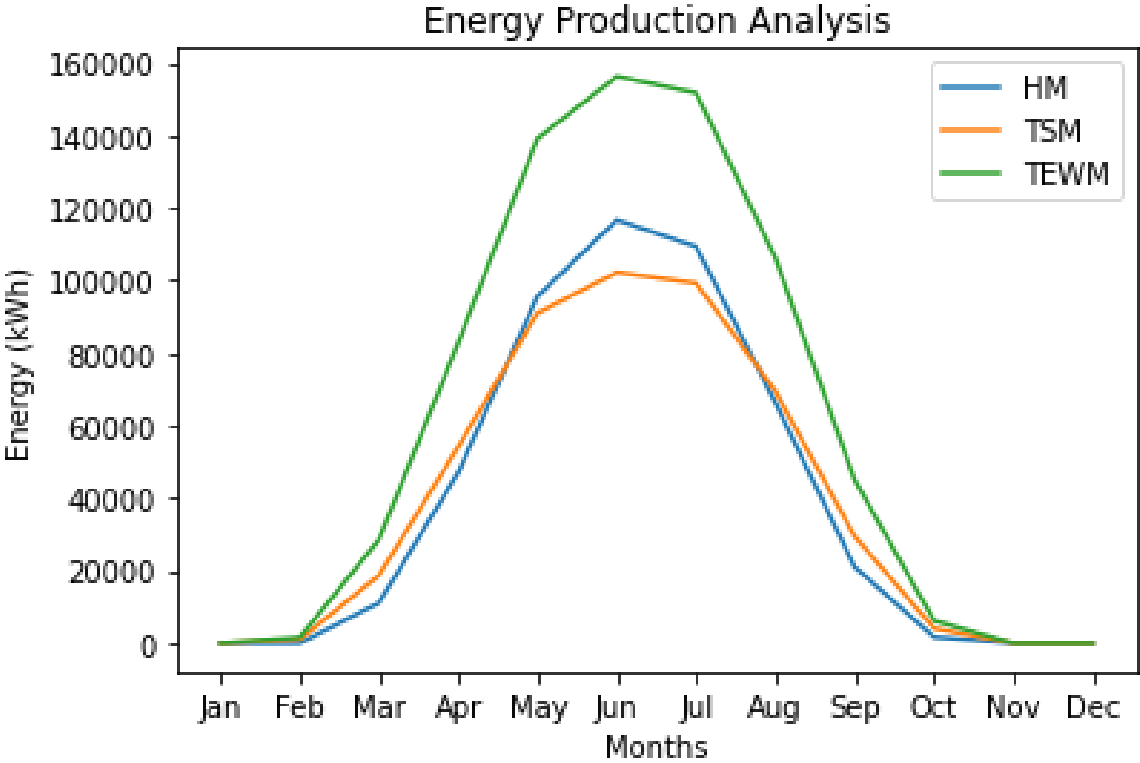
Figure 24: Monthly energy production (kWh) for the systems containing horizontal modules (HM), 40° tilted south orientated modules (TSM), and 40° tilted east- west orientated modules (TEWM). The respective annual productions for HM, TSM and TEWM are 469,2 MWh, 469,8 MWh, and 718,2 MWh.

3.6 Warehouse Consumption Covered by the PV Systems

To compare the PV produced energy with consumed electricity from the warehouse, a Python program is used in combination with the results from section 3.5. The program divides the monthly production for a given PV system with the monthly power consumption from the warehouse for each month of the yeas. Figure 25 presents the result in form of three different graphs, showing the percentage of consumption covered by the respective PV system. The TEWM are closest to meet the warehouse electricity demand by covering 25% of the annual consumption, whereas both HM and TSM covers 16%. Due to Tromsø's solar radiation conditions, mentioned in section 2.6, all the systems reach peak production in June, and have insignificant production from November to February.
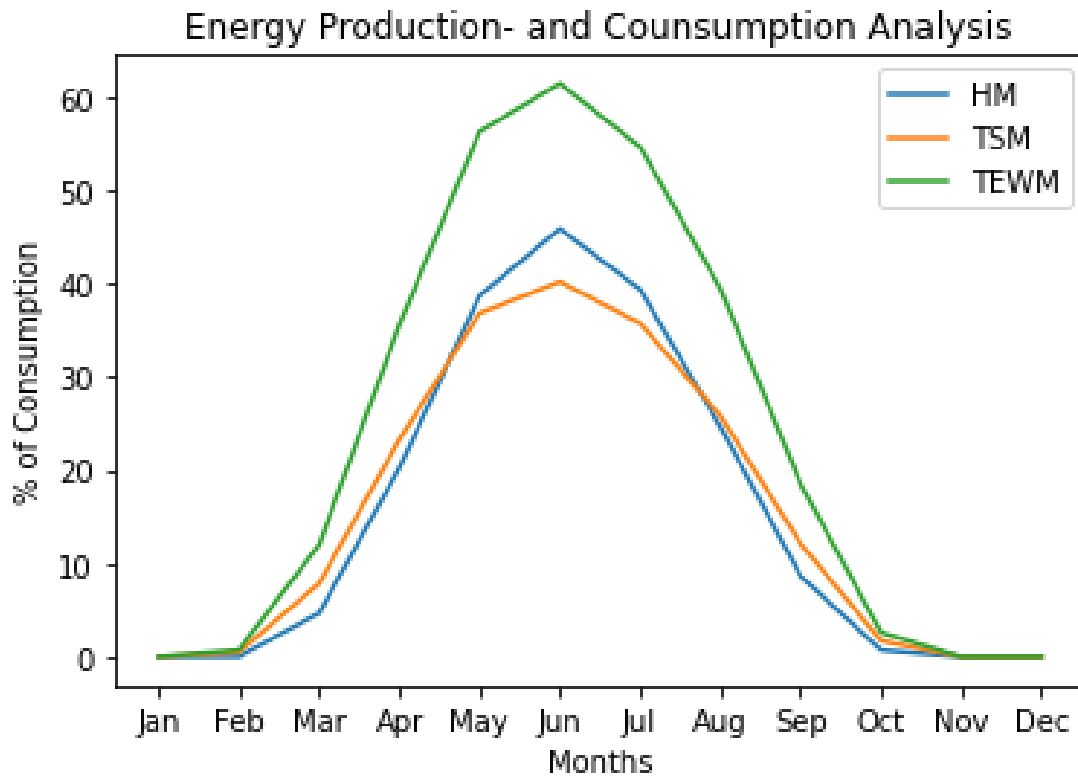
Figure 25: Percentage of the warehouse energy consumption that is covered. The systems containing horizontal modules (HM), $40°$ tilted south orientated modules (TSM), and $40°$ tilted east- west orientated modules (TEWM). TEWM are closest to meet the warehouse electricity demand by covering 25% of the annual consumption, whereas both HM and TSM covers 16%.

3.7 Design of an East- West Orientated PV System

Among the three PV systems presented in section 3.3, results from section 3.5 estimate the system containing TEWM to produce the most. In the following section, further investigation is performed by designing the respective system. The PV system in this study is designed to utilize the maximum of available roof area for module installation, as the warehouse always consumes all PV produced energy due to its high electricity demand.

3.7.1 Inverters and Modules

Choosing the inverters for the PV system, the module provided DC power is used as a base and recommendations regarding the inverter load ratio from section 2.9.1 is followed. The inverter chosen for the system is an ABB PVS- 100 string inverter with a rated input power of 100 kW. To optimize energy production in even shading situations, the inverter contains six MPPTs,

38

each with four string inputs, leading to a total of 24 separate strings to be connected. The inverter provides a three phase, 400 V AC output with a frequency of 50 Hz, matching the existing power supply. DC/AC disconnection, surge protection and fuses are integrated, and for communication with other components in the PV system, Wi- Fi and two ethernet ports are available. To provide sufficient power for the PV system, 12 ABB inverters are chosen, providing a total nominal AC power of 1200 kW and an inverter load ratio of 1,15. Combining all the inverters, 72 MPPT with a total of 288 string inputs are available for disposal. Table 6 contains additional information about the inverter. The chosen module is called SunPower Max3- 400. Each module contains of 104 monocrystalline solar cells, able to provide a nominal power of 400 W. During standard test conditions the module has an efficiency of 22,5%. Additional information about the module is presented in Table 5.

Table 5: SunPower Max3- 400 PV module data sheet

SunPower Max3- 400 PV module	
Nominal power	400 W
Rated voltage (V_{mpp})	65,8 V
Open circuit voltage (V_{oc})	75,6 V
Maximum system voltage	1000 V
Rated current $\left(I_{mpp}\right)$	6,08 A
Short circuit current (I_{sc})	6,58 A
Module efficiency	22,5%
Number of solar cells	104
Module area	1,77 m^2

Table 6: ABB PVS- 100 multi string inverter data sheet

ABB PVS- 100 string inverter	
Input	
Rated input power (DC)	102 000 W
Input voltage range (DC)	360- 1000 V
MPPT input voltage range (DC)	480- 850 V
Number of MPPTs	6
Number of string inputs for each MPPT	4
Maximum DC input current for each MPPT	36 A
Output	
Rated output power (AC)	100 000 W
AC Grid connection type	Three phase, 4W+PE
Rated grid voltage (AC)	400 V
Rated grid frequency	50 Hz
Maximum output current (AC)	145 A
Maximum AC cable cross section	185 mm^2
Maximum efficiency	98,4%

3.7.2 String Calculation

The number of modules in each string is found with the purpose of keeping the string voltage within the inverters input voltage range at all times of significant production. As the string voltage is affected by the ambient temperature, calculations are done with heat- and cold records in Tromsø to find the string voltages in both cases, collected from seklima.met.no. Even though heat and cold records rarely occur, they are used as a basis to ensure designing a PV system suitable for Tromsø's climate. As the voltage increases when temperature drops, the cold record is used in Equation (2) to find the maximum open circuit voltage for a module to be 83,2 V. This voltage is used in Equation (3), resulting in a maximum of 12 modules to be connected in series without surpassing the inverters highest input voltage.

As the module voltage decreases with temperature, the heat record is used in Equation (4) to determine the minimum voltage to be 59,1 V for a module to still maintain production at maximum power point. In addition to including ambient temperature, Equation (4) also contains the parameter T_{add} that considers additional heat due to the installation method. On the base of information provided by Mayfield Energy, the installation method in this study gives an additional temperature of $30°C$. The result from Equation (4) is further used in Equation (5) to calculate that the minimum number of modules in a string must be 7 to keep within the inverter voltage range in hot periods. Using these calculations as a basis, a string length of 12 modules is chosen, giving a voltage range of 710 - 1000 V. This meets the requirements considering the inverter input voltage range. Results regarding string calculations are presented in Table 7 while the complete calculation is presented in Appendix B. The complete PV system is presented in Table 8, and contains of 3456 modules divided into 288 strings, providing a peak power of 1382 kW DC. For transfer to alternating current, 12 inverters with a total of 288 string inputs are chosen, giving a nominal power of 1200 kW and a ILR of 1,15.

Table 7: String calculation

Sting calculation	
Maximum module open circuit voltage ($V_{OC,max}$)	83,2 V
Minimum module voltage at maximum power point ($V_{MPP,min}$)	59,1 V
Rated module voltage	65,8 V
Maximum number of modules per string	12
Minimum number of modules per string	7
Minimum ambient temperature	$-18\,°C$
Maximum ambient temperature	$30,2\,°C$
Chosen number of modules per string	12
Maximum string open circuit voltage ($V_{OC,max}$)	1000 V
Minimum string voltage at maximum power point ($V_{MPP,min}$)	710 V
Rated string voltage (V_{mpp})	790 V
Inverter input voltage range	360 V- 1000 V

Table 8: PV system design. The system and contains of 3456 modules divided into 288 strings, providing a peak power of 1382 kW DC. For transfer to alternating current, 12 inverters with a total of 288 string inputs are chosen, giving a nominal power of 1200 kW and a ILR of 1,15.

PV system design	
One string	
Modules connected	12 modules connected in series
One inverter	
Modules connected	288 modules divided into 24 strings
Inverter	6 MPPT's with 4 inputs each, 24 inputs total
Total PV system	
Modules connected	3456 modules divided into 288 strings
Inverter	12 inverters with a total of 288 inputs
Nominal power from all inverters	1200 kW
Nominal power from all modules	1382 kWp
Inverter load ratio (ILR)	1,15

3.7.3 Cable Calculations

Table 21, located in Appendix A , and aspects described in section 2.9.2 is used in the process of determining sufficient CCC for cables involved in the PV system. Method E is the selected method of installation for both AC and DC cables, representing installation on a cable tray. Cable trays offers air circulation for the cables, are easy installed, and can handle the large number of cables containing in the PV system. As the CCCs in Table 21 only is valid for ambient temperatures below 30℃, a correction factor must be added in cases of surpassing temperatures. Temperature data for the location shows that no such measure is needed, as the ambient temperatures never exceed the reference value, neither outside nor inside the technical room. Further, the sufficient cross section chosen from Table 21 is controlled to be within the range of acceptable voltage drop using Equation (11). As the CCC for a cable decrease with voltage, the lowest string voltage possible to obtain at maximum power point production is used as reference value to ensure sufficient cross section despite low voltages from the modules. For AC cables connecting the inverters to the grid, the inverter output voltage is use as reference

value. For AC power transmission, an aluminium cable with a cross section of 95 mm^2 is chosen. Method of installation and eventual correction factors considered, the cable has a CCC of 183 A, which sufficiently handles the inverter output current and exceeds the minimum cross section requirement to avoid voltage drop. For DC power transmission, a copper cable with the cross section of 2,5 mm^2 and a CCC of 23 A is chosen by the same approach. Table 9 presents a summary of the cable calculations whereas detailed calculations are presented in Appendix A. Figure 26 presents a schematic diagram of one string connected to an inverter, including both AC and DC cables.

The AC cable length is constant as all inverters are mounted in the same location, with equal distance to the main switchboard. In total, 1920 m of AC cables is used, divided into 48 cables with individual lengths of 40 m. Each of the three module rows in Figure 16 have an individual distance to the inverter room, leading to individual lengths for the DC cables connecting the strings and inverter. Rows 1, 2, and 3 respectively has 100, 60, and 100 meters to the technical room. Lengths for the AC and the DC cables are presented in Table 10 and Table 11.

Table 9: Sizing of AC and DC cables involved in the PV system on Coop's roof.

Cable Sizing	AC cable	DC cable
Method of installation	Cable Tray	Cable Tray
Correction factor due to ambient temperature	1,0	1,0
Correction factor due to distance between cables	1,0	1,0
Cable length (m)	40	10
Minimum current carrying capacity required (A)	145	6,58
Minimum cross section to avoid voltage drop (mm^2)	66	0,68
Selected cross section (mm^2)	95 Al	2,5 Cu
Current carrying capacity of selected cross section (A)	183	23

2 * 2,5 mm^2 Cu cable for DC power transmission

4 * 95 mm^2 Al cable for AC power transmission

Module- SunPower 400 W

Inverter- ABB 100 kW
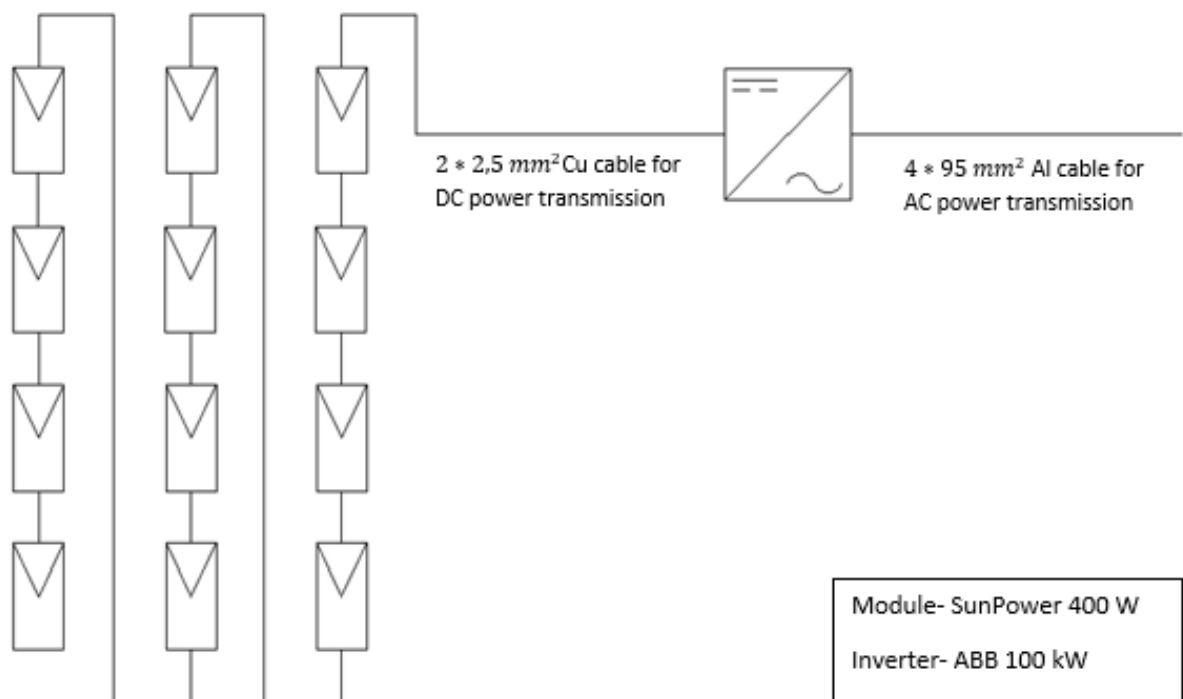
Figure 26: Schematic diagram of one string connected to the inverter. The scheme includes the DC cable connecting the string and inverter, and the AC cable connecting the inverter and main switchboard.

Table 10: Length of AC cables involved in the PV system on Coop's roof.

Length of AC cables	
One inverter	
Number of AC cables	4
Individual cable length	40 m
Total system	
Number of AC cables	48, divided into 12 inverters
Meters of AC cable needed	1920 m

Table 11: Length of DC cables involved in the PV system on Coop's roof.

Length of DC cables	
Row 1	
Number of DC cables	24 for each of the four inverters, 96 in total
Individual cable length	100 m
Row 2	
Number of DC cables	24 for each of the four inverters, 96 in total
Individual cable length	60 m
Row 3	
Number of DC cables	24 for each of the four inverters, 96 in total
Individual cable length	100 m
Total system	
Meters of AC cable needed	1920 m

3.8 Energy Production and Consumption Analysis

The energy production and consumption analysis predict the warehouse's energy accounts for the future. Due to the module degradation and power efficiency increase, the module production and warehouse consumption respectively decreases with 0,32% and 0,07% per year. Table 12 presents the first three years of energy analysis, whereas the entire analysis is presented in Appendix D.

Table 12: Energy production and consumption analysis, all units in kWh. Due to the module degradation and power efficiency increase, the module production and warehouse consumption respectively decreases with 0,32% and 0,07% per year.

Year	1	2	3
Consumed energy	2 794 035	2 792 079	2 790 125
Produced energy	718 236	715 938	713 647
Energy required from grid	2 075 799	2 076 142	2 076 478

3.9 Economic Analysis of an East- West Orientated PV System

To determine the cost and profitability of the PV system on Coop's roof, an economic analysis is made for the future energy costs with and without a PV system and used in a cashflow analysis to determinate the project's NPV. The analysis evaluates results from the energy consumption- and production analysis, as well as predictions for Coop's future electricity costs with price rates provided by Arva. To investigate how the electricity price affects the profitability, the NPV is calculated for different price rates and presented in a plot.

The cost of the PV system is predicted to reach 5 931 160 NOK and is mostly impacted by the 3456 modules. As presented in Table 13, inverters, fundaments and installation cost also have significantly impact on the system cost. An additional cost is added to consider expenses from various accessories. The future energy prices for Coop, presented in Table 14, is used as a base for the energy cost predictions with and without a PV system, presented in Table 15. Fixed grid rents and power tariffs are assumed values that are equal in both predictions as they are assumed to be independent of the power consumption.

Table 13: Cost of an 40° tilted east west orientated PV system in NOK.

Component	Cost (NOK)	Total cost (NOK)	% Of Total Cost
Modules	1 000 NOK	3 456 000	58
Inverters	48 750 NOK	585 000	10
Fundaments	300 NOK/module	1 036 800	17
AC cables	180 NOK/meter	86 400	1
DC cables	3 NOK/meter	5 760	0,1
Installation	200 NOK/module	691 200	12
Additional costs		70 000	2
Total cost		5 961 160	

Table 14: Energy prices. The electricity cost is predicted by NVE, and the remaining values are collected from Arva.

Energy prices	
Electricity cost (NOK/kWh)	0,46
Energy fond fee (NOK/kWh)	0,01
Grid rent, energy dependent (NOK/kWh)	0,11
Grid rent, consumer fee (NOK/kWh)	0,089
Grid rent, fixed (NOK/year)	711 000

Table 15: Yearly energy cost predictions with and without a PV system

Yearly energy cost (NOK)	Without PV	With PV	Cost saved with PV
Electricity	1 285 256	954 868	330 389
Power peak fee	446 000	446 000	0
Grid rent, fixed	711 000	711 000	0
Grid rent, energy dependent	307 344	228 338	79 006
Grid rent, costumer fee	248 949	184 954	63 995
Energy fond fee	27 940	20 758	7 182
Total yearly cost	3 026 489	2 545 917	480 572

The cash flow analysis in Table 16 considers annual income and expenses with a PV system over a period of three ears, while Appendix E shows the analysis in its entirety. Costs saved from PV produced energy represents the annual income and is collected from Table 15. Energy production decreases constantly due to a yearly module degradation of 0,33%.

Detailed information about the investment cost is described in Table 13 whereas the cost of maintenance and reparation is a constant, annual expenses assumed to be approximately 1% of the investment cost. With the cash flow analysis as a base, the NPV for the PV system is calculated to 1 044 837 NOK and 2 481 203 NOK with the respective rates of 0,46 NOK/kWh and 0,58 NOK/kWh, representing NVE's basic and high price scenarios. The mention results are presented in Figure 27, where the project NPV is plotted as a function of the electricity price. Calculating the NPV, the WACC is set to 4%, and is the following within the value of utility scale PV systems in Europe as mentioned in section 2.9.5.

Table 16: Three years of cash flow analysis for an east west orientated PV system, all values in NOK.

Year	0	1	2
Cost saved from PV produced energy		480 572	479 034
Maintenance and reparations		-58 000	-58 000
Investment cost	-5 961 160		
Result	-5 961 160	422 572	421 034
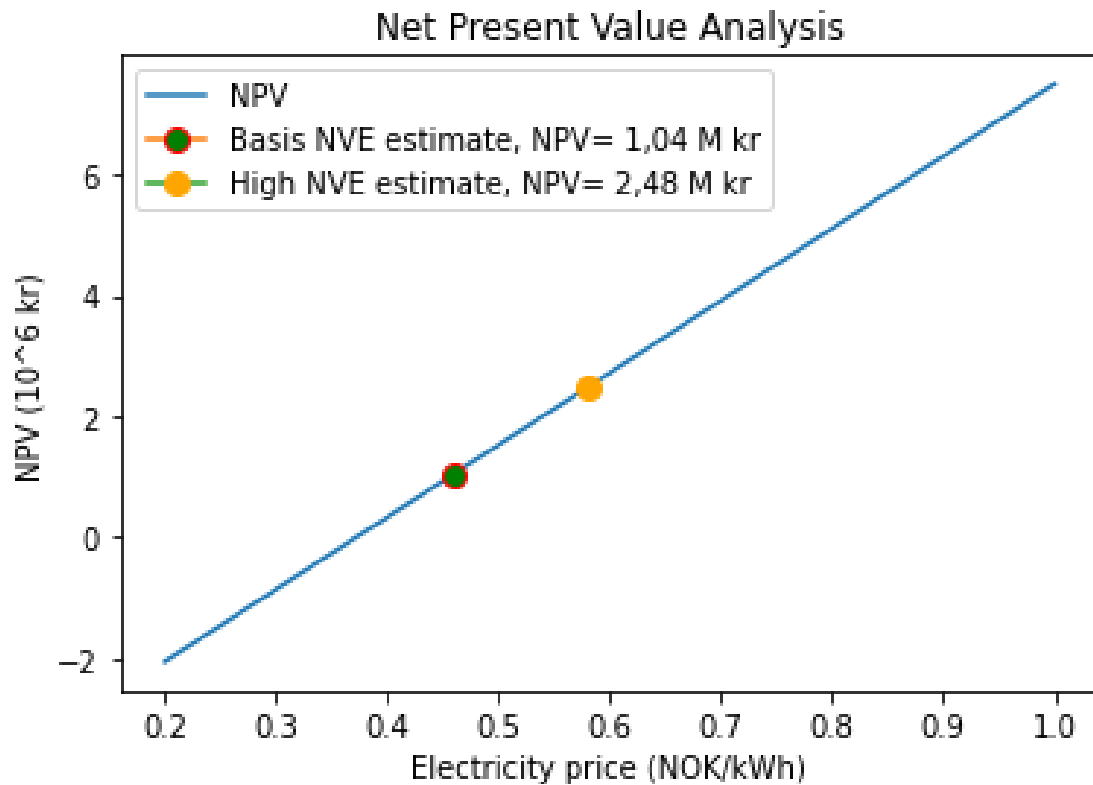
Figure 27: Net present value (NPV) for a PV system as a function of the electricity price. The red and orange markers respectively represent NVE's basis and high price estimates for future electricity, with rates of 0,46 NOK/kWh and 0,58 NOK/kWh.

3.10 Renting Roofs to Meet Coops Electricity Demand

To cover a greater part of the warehouse power consumption, this study considers installing a PV system on the roof of a nearby building and transmit the power to coop with inter- building cables. In addition to finding a solution for covering Coops electricity demand, the objective is to investigate the idea of utilizing otherwise unused roofs on neighbour buildings for solar energy production. As a part of the investigation, it is desired to find a general approach for choosing the most suitable of the neighbour buildings. To do so, finding a roof with common features to Coop's roof is desired as this enables the use of former calculations from the PV system presented in section 3.3. By using similar systems, additional discounts for buying and installing the PV system are assumed. Buildings located within close distances from the main building is preferred, as both the electrical losses and the installation costs increases with distance for the cables transporting electricity between the buildings.

ArcGIS is used to measure distances, areas, solar radiation potential, and to present the chosen neighbour roofs. Figure 28 illustrates the nearby buildings with distances and areas acceptable to be considered for PV system installation. Building 1 and Building 2 have their respective distances of 225 m and 73 m to Coop, and roof areas of 8300 m² and 5300 m².
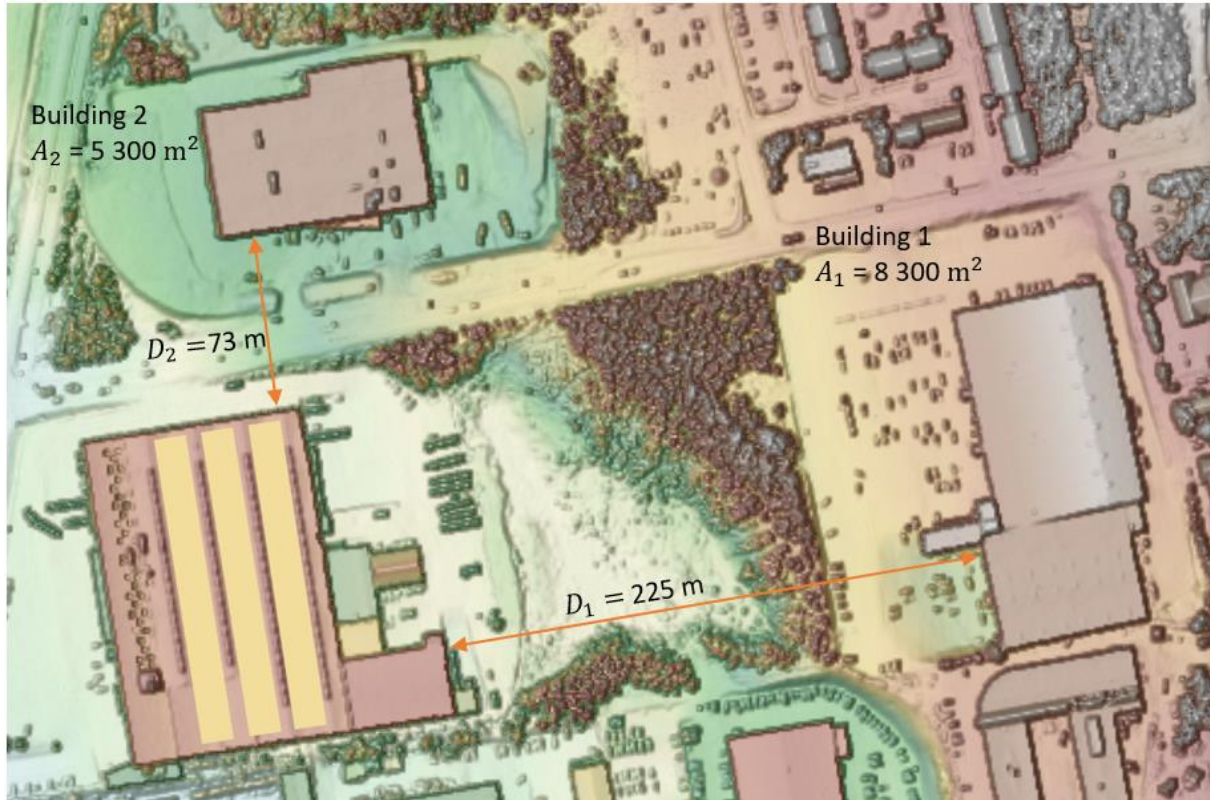
Figure 28: Map of Coop's warehouse with the distances to the nearby buildings, and their respective areas. Building 1 and building 2 have their respective distances of 225 m and 73 m to Coop, and roof areas of 8300 m^2 and 5300 m^2.

3.10.1   The PV System

Among the three installation methods presented in section 3.3, the east- west orientated system is found to be most beneficial to install on a horizontal roof in the given location. Following, the PV system chosen to be installed on Building 1 is identical to the system on Coops roof, presented in section 3.7, whereas the PV system chosen to be installed on building 2 has the same setup but is 30% smaller due to less available roof area. On the quest of reducing stress from the grid, inter building cables are chosen to transmit power back to the warehouse. To determine sufficient cross section for the inter- building cables, the approach described in section 2.9.2 is used and calculations are shown in Appendix A. To find the cost of buying and installing the cables in a trench, prices from a local contractor are used to ensure a realistic

approach. AC cables from the inverters are collected in a switchboard in the neighbour building, and larger cables suited for longer lengths are used between the buildings. For each cable, it is assumed an additional length of 75 meters to the inter- building distance presented in Figure 28, to reach the main switchboard inside the warehouse. The cable sizing results are presented in Table 17, and shown in Figure 29.

Table 17: Sizing of the AC cables between Coop and Building 1 (CB1), and between Coop and Building 2 (CB2)

Cable Sizing	C+B1 AC cable	C+B2 AC cable
Method of installation	Cable Trench	Cable trench
Correction factor, ambient temperature	1,0	1,0
Correction factor, distance between cables	1,0	1,0
Cable length (m)	300	148
Minimum current carrying capacity required (A)	1 740	1 392
Minimum cables needed to avoid voltage drop	5	2
Selected cross section (mm^2)	240 Al	240 Al
Current carrying capacity of selected cross section (A)	250	250
Number of cables needed	7	6
Total current carrying capacity	1 750	1 500
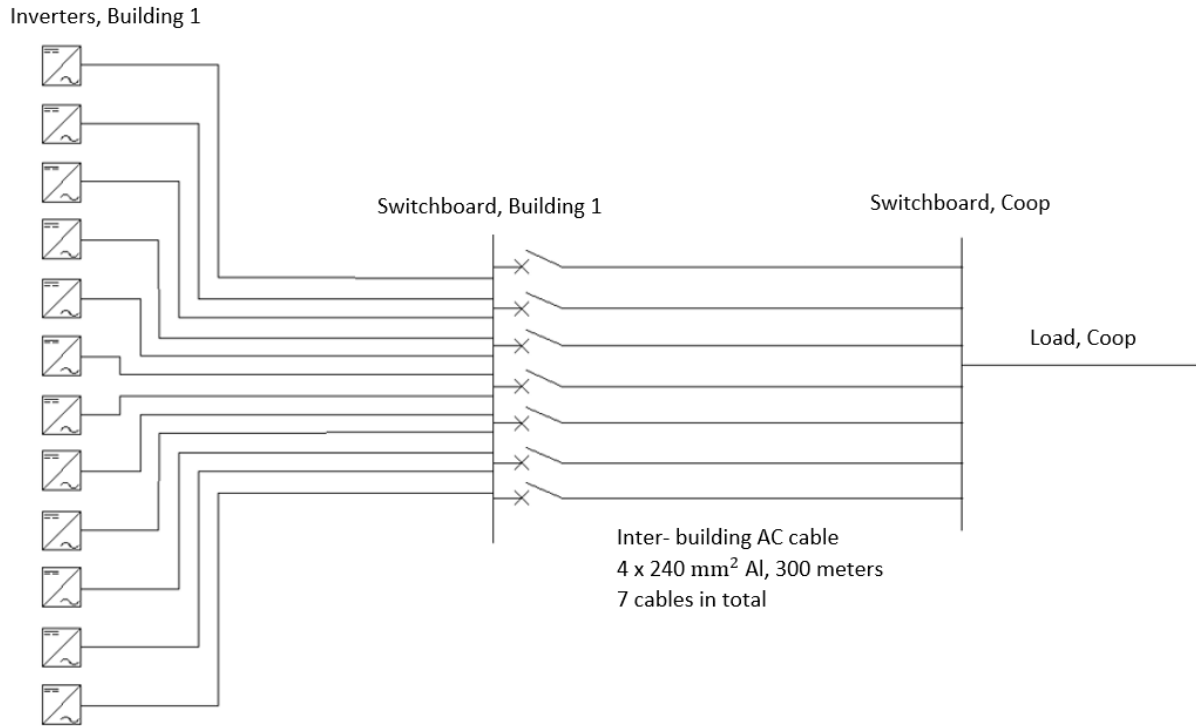
Figure 29: Schematic diagram of the inverters and switchboard in Building 1, and the inter- building AC cables connecting Building 1's PV system to Coops switchboard.

3.10.2   Energy Production Analysis

Three years of an energy production and consumption analysis are presented in Table 18 for the system on Coop, the system on Coop and Building 1 (C+B1), and the system on Coop and Building 2 (C+B2), whereas the complete analysis is presented in Appendix F. Compared to the PV system on Coop, C+B1 produces twice the energy. As building 2 has 20% less available roof are compared to building 1, the C+B2 system produces less. Figure 30 corresponds to the results of Table 18 and presents the percentage of Coops energy consumption covered by the systems. The systems on Coop, C+B1 and C+B2 respectively covers 25%, 50% and 44% of the annual warehouse power consumption.

Table 18: Energy production and consumption analysis for the systems on Coop, Coop and Building 1, and Coop and Building 2 with all values in kWh.

Year	1	2	3
Consumed energy by Coop	2 794 035	2 792 079	2 790 125
Coop			
Produced energy	718 236	729 658	727 323
Energy required from grid	2 062 035	2 062 422	2 062 802
Coop and Building 1			
Produced energy	1 436 472	1 431 875	1 427 293
Energy required from grid	1 357 563	1 360 204	1 362 831
Coop and Building 2			
Produced energy	1 221 001	1 217 094	1 213 199
Energy required from grid	1 573 034	1 574 985	1 576 925
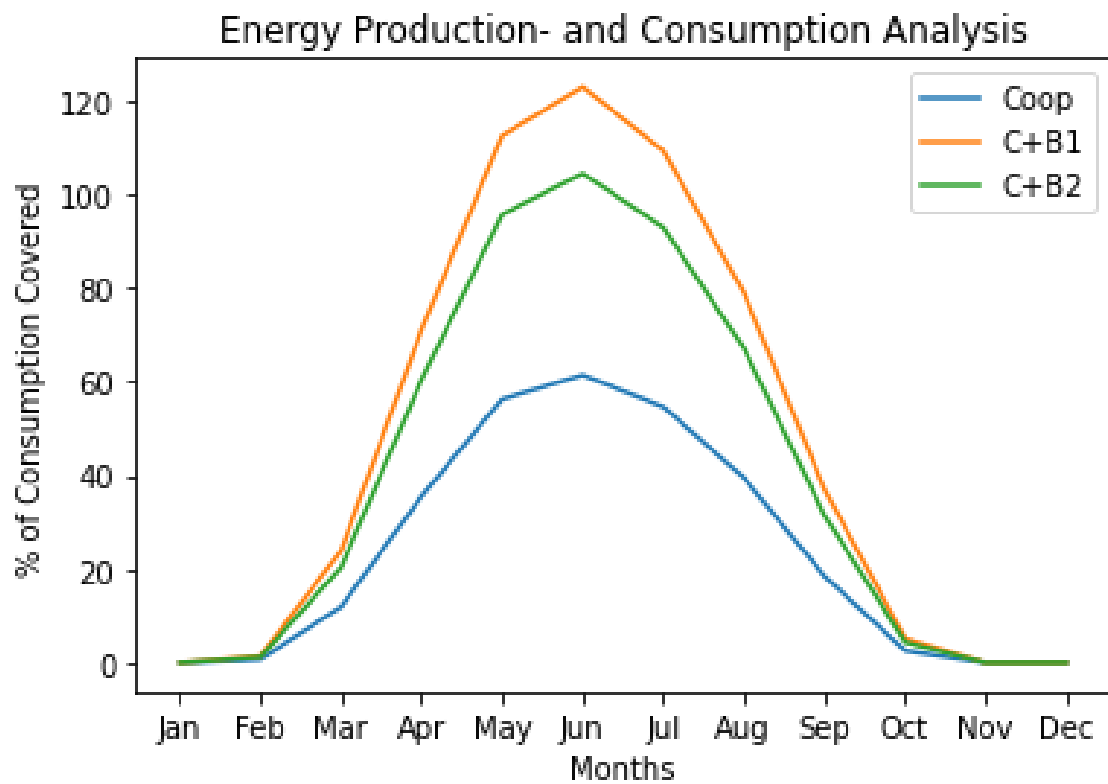
Figure 30: Percent of Coops energy consumption covered by PV produced electricity. The systems Coop, Coop and building 1 (C+B1), and Coop and building 2 (C+B2) respectively covers 25%, 50% and 44% of the annual consumption.

3.10.3   Economic Analysis

As the quantity of system components heavily increases with the systems on C+B1 and C+B2, an additional discount of 10% is assumed to the prices presented for Coops system in Table 13. The cost of the systems, including additional discounts and the inter- building cables is presented in Table 19. For the system on C+B1, inter- building cables entails an additional cost of 969 600 NOK compared to the corresponding cables in the C+B2 system, as the buildings, presented in Figure 28, are located with a greater distance.

The system cost along with annual income and expenses for the systems on C+B1 and C+B2 are presented in the cash flow analysis in Table 20. For both systems, the annual income decreases in time due to a yearly module degradation of 0,33%, whereas the maintenance and reparation cost is a constant, annual expense assumed to be 1% of the investment from Table 19. An additional expense is incurred as the owner of each neighbour building is paid 20% of the annual profit from the respective PV system as rent. An additional cost is added for both systems to consider expenses from various accessories. As the system on C+B1 has the greatest power output, both annual income and investment cost surpasses the system on C+B2. The cash flow analysis in Table 20 is presented over a period of three ears, while Appendix F shows the analysis in its entirety.

Results from the analysis are used to determine net present values for the systems on Coop, C+B1 and C+B2. The systems respectively break even at 0,37 NOK/kWh, 0,55 NOK/kwh and 0,50 NOK/kWh, as shown in Figure 31. Despite both the systems which includes a neighbour roof depends on a higher electricity price to break even, they simultaneously become more profitable than Coop for prices surpassing 0,9 NOK/kWh. Up against each other, the system on C+B2 are more profitable than C+B1 until this point, as C+B1 has the highest investment cost, and the following a higher dependency on the electricity price to break even. For prices above 0,9 NOK/kWh, C+B1 is the most profitable system of all.

Table 19: Individual cost for the system components, and the total cost for the PV systems on Coop and Building 1(C+B1) and Coop and building 2 (C+B2). Building 2 has a 20% smaller system than the building 1, resulting in a reduced system cost.

Component	Individual Cost	C+B1	C+B2
Modules	900 NOK	6 220 800	5 287 680
Inverters	43 875 NOK	1 053 000	895 050
Fundaments	270 NOK/ module	1 866 240	1 586 304
AC cables	162 NOK/ meter	155 520	155 520
DC cables	2,7 NOK/ meter	10 368	10 368
Inter- building cables	800 NOK/ meter	1 680 000	710 400
Installation	180 NOK/ module	1 244 160	1 057 536
Additional cost		200 000	170 000
Total cost		12 430 088	9 872 858

Table 20: Cash flow analysis for the systems on Coop and building 1 (C+B1) and Coop and building 2 (C+B2) in NOK.

Year	0	1	2
Coop and Building 1			
Cost saved from PV produced energy		1 593 191	1 588 093
Maintenance and reparations		-124 300	-124 300
Rent to building owner		-318 638	-317 618
Investment cost	-12 430 088		
Result	-12 430 088	1 150 252	1 146 173
Coop and Building 2			
Cost saved from PV produced energy		1 354 212	1 349 879
Maintenance and reparations		-98 729	-98 729
Rent to building owner		-270 842	-269 975
Investment cost	-9 872 858		
Result	-9 872 858	984 641	981 175
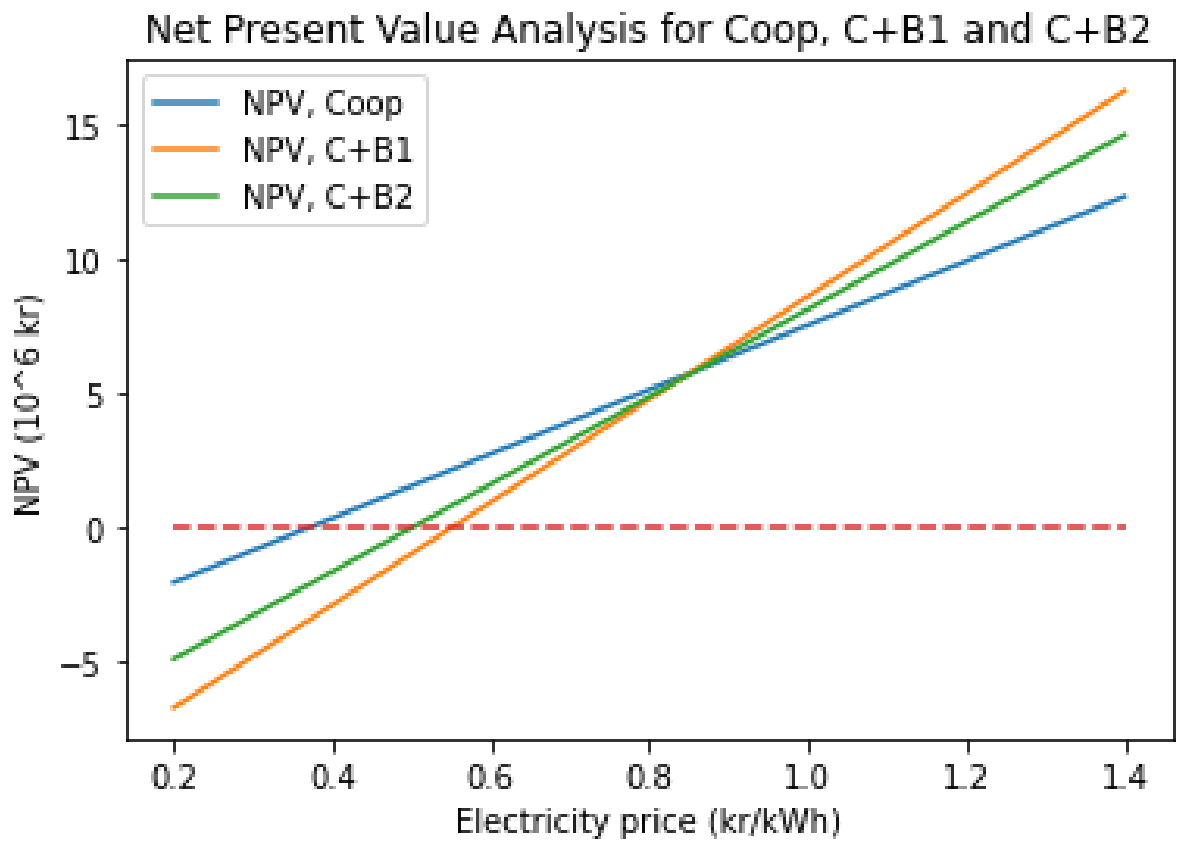
Figure 31: Net present value (NPV) analysis for the PV systems on Coop, Coop and Building 1 (C+B1), and Coop and Building 2 (C+B2).

4 Discussion

4.1.1 Consumption

As shown section 3.6, the energy consumption for the warehouse correlates with temperature, leading to higher energy demand in the summer months. As mentioned in section 2.6 and confirmed in section 3.4, incoming radiation in Tromsø also reaches its maximum in this period. The increase in module produced electricity during same period as the electricity demand peaks, makes it interesting to perform further investigations regarding PV installation on the warehouse roof. Additionally, the efficiency and temperature correlation, mentioned in section 2.2.2 makes Tromsø an interesting destination for PV module installation.

4.1.2 Area Utilization

Not all the warehouse roof is suitable for module installation, due to objects such as fans and ventilators. To avoid conflict, the assigned area for module installation maintains proper distances to the mentioned obstacles. As presented in Figure 16, the area forms three columns with a symmetric design, intending to simplify calculations regarding solar radiation, power production, and shadowing.

Regarding utilization of the given roof area in section 3.2, the objective is to ensure maximum yield in the high- radiation period occurring from May to July. For the two systems with tilted modules, row spacing is adapted to limit shadowing in this period, as presented in section 3.3.2 and 3.3.3. Outside the high radiation period, such design cause times of shadowing between modules, as the row spacing is not adapted to the decreased solar elevation angle. Despite times of shadowing, the modules still maintain a certain production during spring and fall. By assuming a conservative approach and design the system to avoid shadowing during all months with significant production, the module row spacing must be increased. Compared to the row spacing of 1,29 meters needed to limit shadowing between May and July, a distance of 4,1 meters is required to avoid shadowing from March to September. Such increase would reduce the number of modules by approximately 50%, and despite higher harvesting in spring and fall, less of the radiation peaks will be utilized during summer, resulting in a decrease in the overall energy production. Due to the module row spacing, TSM covers the least area with modules

whereas HM, on the other hand, offers higher area utilization as there is no shadowing from other modules to consider. TEWM have the greatest area utilization as they are mounted to a triangle shaped stand facing both east and west, as shown in Figure 18. The otherwise unused area behind a tilted module to avoid shadowing, is filled with an additional module as presented in section 3.3.3. Despite the west- orientated modules experiencing shadowing in the morning, the east orientated modules will have solar radiation during the same time. At the second half of the day, the east orientated modules will experience shadowing as the west orientated modules have solar radiation. Compared to TSM, TEWM therefore utilizes a significantly higher amount of the area, despite having the same module row spacing.

4.1.3 Solar Radiation Potential

To determine solar radiation potential per square meter for the three installations investigated in this study, PVsyst and ArcGIS results are compared in section 3.4.3. The comparison shows that PVsyst generally gives higher estimates during the year. As presented in section 2.10, PVsyst uses a combination of different nearby weather stations to calculate the solar radiation on a given location. Satellite data is also used when simulating in remote locations with distances greater than 50 km to nearest ground station. The combination of several ground stations and satellite data may give overestimated simulation results. ArcGIS on the other hand, calculates solar radiation potential for the exact roof area, using the Area Solar Radiation tool. ArcGIS also considers shading caused by the terrain surrounding the location, such as mountains. The PVsyst simulations in this study does not include far shading and may lead to unrealistically high radiation values compared to ArcGIS. In the manuscript "Rethinking the role of solar energy under location specific constrains" (Chiesa, et al., 2020), solar radiation potential in Tromsø is investigated by comparing data from ArcGIS and PVsyst. The study indicates that March and April are the months with especially high estimates, and concludes that despite Meteonorm data is acceptably accurate, PVsyst tends to overestimate the solar radiation potential in Tromsø. This conclusion matches the results from section 3.4.3 in this study, as March and April are the months where the highest differences occur between the simulations. As the solar radiation predictions presented in section 3.4.2 are considered overestimated, it is decided to proceed with radiation results from ArcGIS in further calculations.

As presented in Figure 20, TSM have the highest radiation potential per square meter of the three systems, as the surfaces achieves the most perpendicular angle with the solar rays. Even though the TEWM have the same tilt, they are assumed to harvest 20% less radiation, as orientation causes them to be less perpendicular to the solar rays. As Tromsø's radiation conditions are likely to cause additional losses, the 20% loss factor used in this study surpasses the one mentioned in section 2.6.2 to avoid overestimating. Despite a lower peak, TEWM have higher radiation exposure during morning and afternoon compared to the TSM, as shown in Figure 9. HM have the least radiation intensity, as the module angle deviates most from the ideal angle presented in section 2.7.

4.1.4 Energy Production

Equation (12) is used to calculate the energy production for each system with the respective radiation potentials presented in section 3.4.3. For the two systems with tilt, all modules will not always experience full radiation potential due to shadowing. This deviation especially affects the energy production estimates during spring and fall, as the module row spacing calculations in section 3.3 mainly intends to limit shadowing during summer. As discuss in section 4.1.3, the systems are designed to harvest the most during the high- radiation period in summer, at the expense of energy yield during spring and fall. On the other hand, the overall radiation potential estimated from ArcGIS is conservative, and may be exceeded by the actual radiation. Calculating the energy production, the performance ratio for each system is set to 85%, which classifies them as high- performance PV systems according to section 2.9.3. This value is determined with Tromsø climate as a base, as several aspects of the performance ratio are positively affected by cold temperatures, such as the inverter efficiency and conductivity of cables.

In addition, losses due to shadowing from nearby objects, apart from other modules, are assumed as unlikely since the modules are located on a flat roof with no objects surrounding. As the solar radiation predictions presented in section 3.4.2 are considered overestimated, radiation results from ArcGIS are used with Equation (12) to calculate the energy production in this study.

According to the results in section 3.5, HM and TSM produces the same annual power despite the differences. HM have the least radiation potential of the three systems, but good area utilization as shadowing issues is neglectable. TSM have opposite characteristics, as the modules gains high radiation potential due to tilt and orientation but requires great spacing to avoid shadowing. With more than twice the production, TEWM have the highest energy production of the three systems. The combination of decent radiation values and excellent area utilization able this system to cover 25% of the warehouse' annual power consumption in the same period as the remaining systems cover 16%.

4.1.5 PV System Design

Performing the string calculations in section 3.7, maximum and minimum string length is calculated by using temperatures from cold- and heat records in Tromsø as a basis. These values are considered conservative since temperature records rarely occur. Despite giving less freedom of choice when designing strings, the conservative approach ensures stable power production during all types of climates. In this study, inverters with multiple MPPTs are chosen with the purpose of maintaining the highest energy production possible, despite shadowing. TEWM are particularly vulnerable to shading as the modules are fixed in opposite orientations, increasing the probability for different radiation conditions at the same time. In addition to increasing the power production by using several MPPT's, multi string inverters also offers flexibility when designing a PV system as they are offered in a various range of models. Despite the high number of MPPT, the multi string inverters have disadvantages regarding system complexity and investment costs as mentioned in section 2.9.1. By prioritizing inverter types with high nominal power over the amount of MPPT, a smaller number of inverters could be used. For instance, certain types of central inverters can fully cover a PV systems power demand alone, requiring less complex communication systems between inverters, and lower investment costs.

As presented in section 3.7, the inverter load ratio for the PV system is 1,15 since the AC power output is 15% less than the DC power input. As mentioned in section 2.9.1, an undersized inverter will be sufficient for most hours during the day, as a PV system mostly produces below its nominal power. In addition, smaller inverters lower the investment cost as they cheaper, easier to install, and require smaller AC cables compared to lager inverters. The downside for undersized inverters is power clipping which occurs in times of high-power production from the modules, leading to power losses. Power clipping can be avoided by installing oversized

inverters and following decrease the inverter load ratio below 1. Despite utilizing the power peaks during mid- day, oversized inverters have higher costs and lower utilization of the power produced during low radiation conditions. Power clipping is unlikely to occur using the east-west orientated PV system designed in this study, due to its power production characteristics. Compared to the typical noon peaks occurring with south orientated modules, power production from TEWM is more evenly divided throughout the day, as presented in Figure 9.

In this study, all the 24 inverters are placed inside a technical room under the warehouse roof to increase lifetime and lower the maintenance costs of the components by protecting them from the arctic climate. In addition, short distances between the inverters also gives rise for less complex communication system. Despite the advantages, the room requires indoor space dedicated for the purpose, with a proper cooling system to transport thermal energy emitted from the inverters. To avoid the additional costs and save indoor space, the inverters could be mounted outdoors as they are approved for such installation. Despite the manufacturer's approval for outdoor mounting, such conditions are likely to increase maintenance costs and decrease lifetime due to Tromsø's climate.

4.1.6 Energy Production and Consumption Analysis

The energy production and consumption analysis consider the consumed energy from the warehouse and produced energy from the PV system. While the consumed energy from the warehouse decreases due to the power efficiency increase, the annual power production presented in Table 12 decreases as an effect of the module degradation rate. As mentioned in section 2.5, this rate increases with the ambient temperature as a result of thermal stress. The degradation rate for modules investigated in this study are likely to be positively affected by this phenomenon, due to Tromsøs low temperatures. Despite implementing this effect would give higher energy production estimates, there is a lack of scientific material regarding the subject, and it is the following chosen to use the manufacturer provided rate in this study. The module manufacturer guarantees 92% of the original power production after 25 years, giving a yearly module degradation of 0,32%.

4.1.7 Economic Analysis

Due to the large quantity of components, PV system prices presented in Table 13 includes a discount of 25%, based on information from local wholesalers. The exact discount is unknown as wholesalers in general offers individual agreements based on customer relationships. As changes in the discount rate highly affects the profitability of the project, deviations from the calculated system cost are likely to occur.

For this study, a constant electricity price predicted by NVE is assumed for all the three decades of project duration. As this rate is affected by various factors such as the climate, and both domestic and foreign politics, deviations are likely to occur and must be considered when evaluating the profitability of the PV system. Despite insecurities, much suggests that the prices in Norther Norway's price region, NO4, will rise with time. NO4 has the lowest prices throughout the country as most of the region's produced surplus cannot be transmitted southwards due to grid limitations. Instead, the power is sold cheap to maintain the required power balance in the grid. In time, NVE expects the region's prices to rise as electrification of existing industries and establishing of power consuming factories may reduce the energy surplus. Equinor's desire to electrify their gas plant "Melkøya" in Finnmark within 2027 is one among various examples where electrification of existing industries in Northern Norway is planned (Klo, 2021). Establishments of energy consuming industries are also predicted in Northern Norway, such as Freyr's battery factory in Mo i Rana. Such establishments are likely to rise in the future, as Northern Norway offers industries a sustainable production provided by cheap, renewable energy (Kalkenberg, 2021).

In addition, plans are made for increasing NO4's transmission capacity to utilize the region's energy surplus in remaining price regions instead of selling cheap. Such levelling will result in Northern Norway's electricity prices to rise (NVE, 2021). As NO4 achieves higher transmission capacity to the remaining price regions, it simultaneously becomes affected by the European energy market. Among others, the Russian invasion of Ukraine is an ongoing example of how foreign politics affect the Norwegian electricity prices. Russia usually supplies 40% of the European gas consumption, but due to the war, insecurities regarding Russian gas supply have risen. Such situations impact the European gas market, and subsequently increases the Norwegian electricity prices (Frøjd, 2022).

In addition to the future electricity prices, present electricity cost for Coop is considered. Whereas the total electricity cost and various details are provided by Coop, certain parts are unavailable, such as price rates for grid rent and consumer fees. To present the complete electricity cost in Table 15, remaining price rates are collected from Arva. Note, Coop may have an individual agreement with the grid supplier. As hourly energy consumption data is unavailable for this study, estimates are done to include the additional costs of power tariffs appearing due to consumption peaks. As a result of the mentioned assumptions, certain deviations in the electricity cost might appear. Despite the lack of specifications, the total electricity cost is provided by Coop and considered to ensure realistic estimates.

The economic analysis in section 3.9 states that the PV system is profitable considering NVE's basic price estimate of 0,46 NOK/kWh. In addition to the PV system cost, main elements affecting this result are both the amount of produced energy, and the worth of it. The worth of the produced energy is determined by the electricity price in NO4, which in the present time is the lowest in Norway, as mentioned in section 2.11. As discussed, various arguments indicate a price increase for the future, giving rise for the project to be even more profitable. Decreasing of system prices during the last years contributes to increasing the profitability of PV systems, as lowering the investment cost allows a system to be profitable at lower electricity prices. Further reduction of hardware cost is predicted to continue in the future. (Chiesa, Stefancich, Sgouridis, & Apostoleris, 2019)

4.1.8 Renting Roofs to Meet Coops Electricity Demand

To cover a greater part of Coop's electricity demand with solar energy, this study investigates installing PV systems on nearby buildings and transmit the produced energy back to Coop with inter- building cables. In addition to find a solution for covering Coops electricity demand, it is desired to investigate the general idea of utilizing otherwise unused roofs on neighbouring buildings for solar energy production. Looking into utilization of unused roofs for PV systems seems to be a reasonable quest, as there are various examples of existing land uses which are cleared away to make room for PV systems. Such development frequently causes negative impact on the environment, such as deforestation which affects the wildlife, oxygen production, and carbon absorption provided by trees (Chiesa & Apostoleris, 2019).

As a part of the investigation, it is desired to find an approach for choosing the most suitable of the neighbour buildings. Knowing to prioritize the building area or the inter- building distance is likely to be a common scenario when considering additional PV system installation. Therefore, two buildings are investigated as potential locations. Building 1 has a large area available for module installation but is located with a great distance from Coop. Building 2 on the other hand, is located closer but has less area to use for module installation. As building 1 has sufficient area, it is chosen to install a PV system identical to Coop's system, presented in section 3.7. The PV system on building 2 has similar design but is reduced by 30% to consider the area available for module installation.

By choosing similar systems, an additional discount of 10% for the systems are obtained due to the large quantities of components, as presented in Table 19. On the quest of reducing stress from the grid, inter -building cables are chosen to transmit power back to the warehouse as presented in Figure 29, transmitting by the existing grid is not considered. The expenses from buying and installing the inter- building cables respectively represent 13% and 7% of the total system cost for C+B1 and C+B2. To be compensated for usage of the roof, the owner of each neighbour building is paid 20% of the annual profit from the respective PV system as rent. This agreement is intended to be fair for both parts, as the neighbour building owner gets to be a part of the price development.

After the project duration of 30 years ends, there are a various range of opportunities for handling the PV system. Dependent on the impact of module degradation, the system might be producing significantly amounts of power after the 30 years, giving rise for the agreement to continue. The building owner buy the system is an additional solution, leading to an income after project end. This study assumes the building owner to take over the system but does not include any income form such agreement.

As presented in Figure 30, the power production for C+B1 covers 50% of the warehouse's annual electricity demand, twice the amount compared to using Coop's system alone. For May, June and July, all the warehouse's demand are estimated to be covered. The production for C+B2 is slightly less, due to the reduced area on Building 2. In terms of economic, neither of the neighbour building systems are profitable by assuming NVE's price estimate of 0,46 NOK/kWh, leaving the system on Coop as the best choice with a NPV of 1 044 000 NOK. Despite a higher break- even point, C+B1 and C+B2 starts being more profitable than a PV system on Coop alone at 0,9 NOK/kWh. These results show that the systems on C+B1 and

C+B2 are more sensitive to changes in the electricity price than Coop, and the following more profitable in periods of high prices, and more likely to run a deficit during periods of low prices. Up against each other, the system on C+B2 reaches profitability at a lower price than C+B1, as C+B1 has the highest investment cost, and the following a higher dependency on the electricity price to break even. For prices above 0,9 NOK/kWh, C+B1 is the most profitable system of all due to the large energy production.

5 Conclusion

This study desires to put attention to less frequent locations in terms of power generation from solar resources by looking at three types of utility scale PV systems to install on the roof of a warehouse in Tromsø, with the purpose of relieve the grid and decrease energy cost for Coop. The area to be filled with modules varies among the systems, as module row spacing is taken into consideration to limit shadowing. Results estimate a row spacing of 1,29 meters to limit shadowing between May and July, while a distance of 4,1 meters is required to avoid shadowing from March to September. The latter proves to decrease the overall energy production as the number of modules is reduced by approximately 50%. Following, it is chosen to limit shadowing between May and July, despite decreased production during spring and fall. Solar radiation potential per square meter is determined for the three systems by comparing estimates from PVsyst and ArcGIS. Results show that PVsyst generally gives higher estimates, and as a similar study concludes PVsyst to overestimate the solar radiation potential in Tromsø it is chosen to proceed with ArcGIS results.

Of the available roof area of 5 460 m^2, HM fills an area of 5187 m^2 as there are no shadowing issues to affect the module spacing. This system receives least solar radiation of all as the solar ray's strike with a less perpendicular angle compared to tilted modules and following covers 16% of the warehouse electricity demand. The system with TSM only utilizes 3210 m^2 for module installation, as great parts of the roof are needed for row spacing to avoid shadowing. Despite achieving the highest solar radiation potential of all due to the ideal tilt and orientation, this system comes out equally as the horizontal in terms of energy production. TEWM fills an area of 6134 m^2, as opposite orientated modules are placed in the otherwise unused spaces required to avoid shadowing. Despite moderate radiation values, this system covers 25% of the electricity demand due to proper area utilization. Being capable of producing the most energy, system design and an economic analysis is performed for the east-west orientated system.

The system consists of 3456 modules divided into 288 strings, with a combined power of 1382 kWp. By using 12 multi string inverters with a total of 288 string inputs and 72 MPPTs, the nominal power reaches 1200 kW AC. Following, the inverter load radio is 1,15, as slightly undersized inverters prove to be sufficient for most hours during a year since PV systems mostly produces below its nominal power. Inverters with multiple MPPTs are prioritized to ensure

maximum production during shadowing, as such phenomenon is likely to occur during spring and fall due to the mentioned module row spacing. The annual module degradation rate is set to 0,33% to match the manufacturers power production warranty but might decrease further as Tromsø's low temperatures reduces thermal stress on the modules. In lack of scientific material regarding the subject, the manufacturer provided rate is used. The system is predicted to cover 718 MWh of the warehouse' yearly consumption of 2 794 MWh.

On the pursuit of covering the most of Coop's power consumption with solar energy, this study investigates installing PV systems on nearby buildings and transmit the produced energy back to Coop with inter- building cables. To determine which affect the most, inter- building distance or available roof area, two buildings with differences in the mentioned properties are considered. Building 1 has an available area of 8 300 m^2 for module installation, and is located 225 m from Coop, whereas building 2 is located at 73 m but only have 5 300 m^2 area to disposal. Of the two buildings, results prove Building 2 to be the best choice for electricity prices below of 0,9 NOK/kWh. For prices above this limit, building 1 gives the most profitability of all systems. By assuming NVE's estimated price of 0,46 NOK/kWh, neither of the neighbour building systems are profitable, leaving the system on Coop as the best choice with a NPV of 1 044 000 NOK. By considering NVE's highest estimate of 0,58 NOK/kWh, the systems on C+B1 and C+B2 breaks even, but the system on Coop's roof still gains the most profit.

For this study, a constant electricity price of 0,46 NOK/kWh is assumed for all the three decades of project duration, predicted by NVE. The profitability of all systems is highly affected by the electricity price, a rate which is impacted by factors such as the climate, and both domestic and foreign politics. Despite insecurities, much suggests that the prices in Norther Norway will rise with time, as a result of increased power demand triggered by electrification of fossil powered industries. In addition, plans are made for increasing the transmission capacity between NO4 and remaining regions, making Northern Norway more affectable by the European energy market.

To end with, this study proves that despite the highly seasonal solar availability, locally produced energy from solar resources in Tromsø can relieve the grid from significant amounts of the additional power consumption predicted to occur in the future. Installing a PV system on a single building turns out to be profitable with the future electricity prices. By installing additional PV systems on the roof of a neighbour building it is proven a doubling in power

production and is additionally allowing power production to coexist with our environment, as locations with no other land uses are utilized. Despite such systems relieves load from the grid, they require larger investment cost and is the following not profitable with the future electricity price assumed in this study.

6 Further work

Due to limitations in time and resources, aspects likely to improve the approach and results of this thesis remain left to be considered for further work. Of the mentioned aspects is an investigation of implementing a load management system to disturb the warehouse energy consumption more evenly thorough the day. After temperature regulation, charging of forklifts are likely to represent a major part of Coop's power consumption. Most forklifts are put to charge in the afternoon and are fully charged during a few hours despite not being used until next morning. By utilizing a load management system, the charging could be awaited to outside the afternoon peaks on the grid. A such system could relieve power peaks from the grid, and lower the cost of power tariffs for Coop.

To ensure maximal utilization during times of low solar elevation angles, vertically mounted modules on the south wall of the warehouse could be considered. Compared to modules with lower tilt angles, vertically mounted modules offer increased energy yield during spring and fall in Tromsø, as they maintain a more perpendicular angle to the solar rays.

A constant module efficiency is chosen for this study. For further work, implementing a variating efficiency that changes as a function of the ambient temperature could lead to higher production estimates as the efficiency is likely to increase as a result of the low temperatures in Tromsø. The performance ratio is assumed equal for the three installations in this study but is unique for most installations in real life. By deriving individual performance ratios for each installation, more correct predictions could be given.

Bibliography

The study "Solar Photovoltaics in Tromsø" and "Solar Photovoltaic Potential on a Warehouse Roof in Tromsø" is previous study of mine. Parts of those studies are used as a base when creating this thesis.

Afework, B., YYelland, B., & Donev, J. (2018, 06 25). *Solar Cell Efficiency*. Hentet fra Energy Education: https://energyeducation.ca/encyclopedia/Solar_cell_efficiency

ArcGIS Pro. (2021). *Spatial Analyst toolbox*. Hentet fra ArcGIS Pro: https://pro.arcgis.com/en/pro-app/latest/tool-reference/spatial-analyst/area-solar-radiation.htm

BEREC. (2017). *BEREC Report Regulatory Accounting in Practice 2017*. Hentet fra Berec: https://berec.europa.eu/eng/document_register/subject_matter/berec/reports/7316-berec-report-regulatory-accounting-in-practice-2017

Bromberg, D. (2021, 04 14). *Choosing the right size solar inverter*. Hentet fra AuroraSolar: https://www.aurorasolar.com/blog/choosing-the-right-size-inverter-for-your-solar-design-a-primer-on-inverter-clipping/

Carl, C. (2014). *Calculating solar photovoltaic potential on residential rooftops in Kailua Kona, Hawaii*. Hentet fra USC: https://spatial.usc.edu/wp-content/uploads/formidable/12/Caroline-Carl.pdf

Chandrasiri, S., & Attygalle, M. (2017, 01 01). *Temperature effect on solar photovoltaic power generation* . Hentet fra Research Gate: https://www.researchgate.net/publication/325146765_TEMPERATURE_EFFECT_ON_SOLAR_PHOTO

Chiesa, M., & Apostoleris, H. (2019, 08 26). *High- Concentration Photovoltaics for Dual- Use with Agriculture* . Hentet fra aip.scitation.org : https://aip.scitation.org/doi/pdf/10.1063/1.5124187

Chiesa, M., Apostoleris, H., & Ghaferi, A. A. (2021, 02 23). *What is going on with Middle Eastern solar prices, and what does it mean for the rest of us?* . Hentet fra Wiley: https://onlinelibrary.wiley.com/doi/pdf/10.1002/pip.3414

Chiesa, M., Eikeland, O. F., Apostoleris, H., Santos, S., Ingebrigtsen, K., & Bostrøm, T. (2020, 11 15). *Rethinking the role of solar energy under location specific constraints* . Hentet fra Science direct : https://www.sciencedirect.com/science/article/pii/S0360544220319459?fbclid=IwAR 2nTLSWUo4JFnNavlHTLztzMgD8dOSce2q8QXz3zcy1l8PxtGQXy29uDk8

Chiesa, M., Simpson, L., & Stefancich, M. (2016, 05 10). *Automatc outdoor monitoring system for photovoltaic panels.* Hentet fra osti.gov: https://www.osti.gov/servlets/purl/1257552

Chiesa, M., Stefancich, M., Sgouridis, S., & Apostoleris, H. (2019, 11 11). *Utility solar prices will contribute to drop all over the world even without subsidies* . Hentet fra Nature.com: https://www.nature.com/articles/s41560-019-0481-4

Climate Science Investigations. (2012, 02 12). *Angle of solar radiation and temperature.* Hentet fra Climate science investigations: http://www.ces.fau.edu/nasa/module-3/why-does-temperature-vary/angle-of-the-sun.php

Delphin, I. L. (2018, 10 31). *Midnattsol.* Hentet fra Store Norske Leksikon: https://snl.no/midnattssol

Diehl, A. (2020). *Determining Module Inter-Row Spacing.* Hentet fra CED Greentech: https://www.cedgreentech.com/article/determining-module-inter-row-spacing

Dupin, R., & Michiorri, A. (2017). *Dynamic line rating forecasting* . Hentet fra Science Direct.

Electrcal Installation wiki . (2021, 08 24). *General method for cable sizing.* Hentet fra Electrical Installation wiki: https://www.electrical-installation.org/enwiki/General_method_for_cable_sizing

Electrical Installation by Schneider Electric . (2021, 08 24). *General method for cable sizing* . Hentet fra Electrical Installation : https://www.electrical-installation.org/enwiki/General_method_for_cable_sizing

Energi Norge. (2021). *Strømnettet- vår viktigste infrastruktur for fremtiden.* Hentet fra Energi Norge : https://www.energinorge.no/fornybarometeret/stromnettet--var-viktigste-infrastruktur-for-fremtiden/

Energifakta Norge. (2021, 08 25). *Energibruken i ulike sektorer*. Hentet fra Energifakta Norge: https://energifaktanorge.no/norsk-energibruk/energibruken-i-ulike-sektorer/

Energy Education Team. (2015, 09 14). *Energy Education Team*. Hentet fra Energy Education Team: http://www.ecogreenelectrical.com/solar.htm

Faranda, R., & Leva, S. (2008, 06). *Energy comparison of MPPT techniques for PV systems*. Hentet fra WSEAS: http://www.wseas.us/e-library/transactions/power/2008/27-545.pdf

Frøjd, K. (2022, 03 01). *Ukraina- konflikten sender norske strømpriser til værs*. Hentet fra TV2.no: https://www.tv2.no/a/14613131/

Gabor, T. (2018). *Power Loss*. Hentet fra Science Direct: https://www.sciencedirect.com/topics/engineering/power-loss

Hanania, J., Stenhouse, K., & Donev, J. (2015, 08 26). *Photovoltaic Effect*. Hentet fra Energy Education: https://energyeducation.ca/encyclopedia/Photovoltaic_effect

Hocken, V. (2021). *What Is Earth's Axial Tilt or Obliquity?* Hentet fra Time and Date.

Hoffmann, T. (2021, 11 08). *SunCalc*. Hentet fra https://www.suncalc.org/#/69.6523,18.9438,8.698683953967338/2021.03.16/09:58/0.7/3

Holmefjord, V., & Kringstad, A. (2019, 03 19). *Et elektrisk Norge- fra fossilt til strøm.* Hentet fra Statnett: https://www.statnett.no/globalassets/for-aktorer-i-kraftsystemet/planer-og-analyser/et-elektrisk-norge--fra-fossilt-til-strom.pdf

Honsberg, C., & Bowden, S. (2020). *Module Structure.* Hentet fra PV Education: https://www.pveducation.org/pvcdrom/modules-and-arrays/module-structure

Honsberg, C., & Bowden, S. (2021). *Solar Radiation on a Tilted Surface*. Hentet fra PV Education: https://www.pveducation.org/pvcdrom/properties-of-sunlight/solar-radiation-on-a-tilted-surface

Honsberg, C., & Bowden, S. (2022). *Degradation and Failure Modes*. Hentet fra PV Education: https://www.pveducation.org/pvcdrom/modules-and-arrays/degradation-and-failure-modes

Honsberg, C., & Bowden, S. (2022). *IV Curve*. Hentet fra PV Education : https://www.pveducation.org/pvcdrom/solar-cell-operation/iv-curve

Honsberg, C., & Bowden, S. (2022). *Open- circuit voltage*. Hentet fra PV Education : https://www.pveducation.org/pvcdrom/solar-cell-operation/open-circuit-voltage

Honsberg, C., & Bowden, S. (2022). *Short- circuit current*. Hentet fra PV Education: https://www.pveducation.org/pvcdrom/solar-cell-operation/short-circuit-current

IEA. (2020). *World Energy Outlook*. Hentet fra IEA: https://www.iea.org/reports/world-energy-outlook-2020

Kalkenberg, L. P. (2021, 11 21). *Ingeniøren Taavi fra Estland skal være med på Norges første batterieventyr.* Hentet fra NRK.no: https://www.nrk.no/nordland/freyr-bygger-norges-forste-batterifabrikk-i-mo-i-rana-1.15686997

Klo, A. (2021, 11 29). *Miljøversting vil elektrifisere Melkøya innen 2027.* Hentet fra NRK.no: https://www.nrk.no/tromsogfinnmark/miljoversting-vil-elektrifisere-melkoya-innen-2027-1.15745097

Li, D. H., Lou, S., & Lam, J. C. (2015). *An Analysis of Global, Direct and Diffuse Solar Radiation*. Hentet fra Science Direct: https://pdf.sciencedirectassets.com/277910/1-s2.0-S1876610215X00130/1-s2.0-S1876610215011674/main.pdf?X-Amz-Security-Token=IQoJb3JpZ2luX2VjEIH%2F%2F%2F%2F%2F%2F%2F%2F%2F%2FwEaCX VzLWVhc3QtMSJHMEUCIQDFgWOMCBHE9xf1jJMmyVts78xqlZ0qhjdHod%2B F8G8SEQIgNfeUDUbsDp

Li, X., Campana, E. P., Li, H., Yan, J., & Zhu, K. (2017, 07). *Energy storage systems for refrigerated warehouses* . Hentet fra Science Direct: https://pdf.sciencedirectassets.com/277910/1-s2.0-S1876610217X00404/1-s2.0-S1876610217364172/main.pdf?X-Amz-Security-Token=IQoJb3JpZ2luX2VjEFwaCXVzLWVhc3QtMSJIMEYCIQCzOgXUHvV4N5F

MFYmCa6fzVT74olCj9cE9MkgtgXAU7AIhANBC2qO0Fk21tntq9jwN%2BraW%2F
rCncy9wKt9mS3me

Mayfield Renewables . (2018, 10 10). *How to calculate PV string size.* Hentet fra Mayfield
Renewables : https://www.mayfield.energy/blog/pv-string-size

Misbrener, K. (2018, 12 13). *How to choose between string and central inverters in utility scale
installations* . Hentet fra Solar Power World:
https://www.solarpowerworldonline.com/2018/12/choose-between-string-and-central-
inverters-utility-scale-solar/

Mow, B. (2018, 04 23). *Lifetime of PV panels* . Hentet fra NREL: https://www.nrel.gov/state-
local-tribal/blog/posts/stat-faqs-part2-lifetime-of-pv-panels.html

Nordahl, H. S. (2012, 06). *Design of Roof PV Installation in Oslo* . Hentet fra NTNU Open:
https://ntnuopen.ntnu.no/ntnu-
xmlui/bitstream/handle/11250/257364/566421_FULLTEXT01.pdf?sequence=1

NVE. (2021, 10). *Langsiktig Kraftmarkedsanalyse, 2021- 2040.* Hentet fra
publikasjoner.nve.no: https://publikasjoner.nve.no/rapport/2021/rapport2021_29.pdf

Pearsall, N. (2017). The Performance of Photovoltaic (PV) Systems. I N.M.Pearsall, *The
Performance of Photovoltaic (PV) Systems, Modelling, Measurement and Assessment*
(ss. 1-19). Elsevier Ltd.

PVsyst. (2022). *Importing meteonorm data.* Hentet fra PVsyst:
https://www.pvsyst.com/help/index.html?meteo_import_meteonorm.htm

PVsyst. (2022). *Meteonorm data and program.* Hentet fra PVsyst:
https://www.pvsyst.com/help/meteo_source_meteonorm.htm?zoom_highlightsub=stoc
hastic

Rensselaer Polytechnic Institute. (2006, 07). *How does that tilt angle and/ or orientation of the
PV panel affect system performance?* Hentet fra
https://www.lrc.rpi.edu/programs/nlpip/lightingAnswers/photovoltaic/14-
photovoltaic-tilt-angle.asp

Rodriguez, L. (2021, 06 01). *Solar panel orientation: How using East- West structures improves the performance of your project* . Hentet fra Rated Power: https://ratedpower.com/blog/solar-panel-orientation/

Rozegnał, B., Albrechtowicz, P., Mamcarz, D., Rerak, M., & Skaza, M. (2021, 3 3). *The Power Losses in Cable Lines Supplying Nonlinear Loads*. Hentet fra Energies.

SMA Solar. (2020, 03 04). *Quality factor for the PV plant* . Hentet fra SMA Solar: https://files.sma.de/downloads/Perfratio-TI-en-11.pdf

Statnett. (2022). *Hvorfor har vi prisområder?* Hentet fra Statnett.no: https://www.statnett.no/om-statnett/bli-bedre-kjent-med-statnett/om-strompriser/fakta-om-prisomrader/

Svarc, J. (2020, 03 20). *Solar Panel Construction* . Hentet fra Clean Energy Reviews : https://www.cleanenergyreviews.info/blog/solar-panel-components-construction

Tayyan, A. A. (2015, 01). *An approach to extract the parameteres of solar cells from their illuminatied $I-$V curves using the Lambert W function.* Hentet fra Research Gate: https://www.researchgate.net/publication/276376570_An_approach_to_extract_the_parameters_of_solar_cells_from_their_illuminated_I-V_curves_using_the_Lambert_W_function

Teknisk Ukeblad. (2021). *Her legges Norges største solcelleanlegg på ett tak* . Hentet fra Teknisk Ukeblad: https://www.tu.no/deltav/energi/annonse-her-legges-norges-storste-solcelleanlegg-pa-ett-tak/514846

The University of Sheffield . (2021). *Comparison of East- West arrays* . Hentet fra Solar Sheffield: https://www.solar.sheffield.ac.uk/panel-data/comparison-of-east-west-arrays/

U.S Energy Information, Administration. (2021, 03 26). *EIA*. Hentet fra Solar Explained, Photovoltaics and Electrcity: https://www.eia.gov/energyexplained/solar/photovoltaics-and-electricity.php.

Åsheim, B. T. (2017, 06). *Analysis of a photovoltaic power plant at Evenstad.* Hentet fra NTNU

Open: https://ntnuopen.ntnu.no/ntnu-

xmlui/bitstream/handle/11250/2454738/17440_FULLTEXT.pdf?sequence=1

Appendix A

To find AC cables with sufficient current carrying capacity for the PV system, the approach described in section 2.9.2 is used. Table 21 presents the most common method of installations for power cables. For each method of installation, the current carrying capacity is given for various cross sections. As an example, the approach of selecting the AC cable connecting the inverter and switchboard is marked. In box 1, method E is chosen as the preferred method of installation, representing multicore cables on cable tray. The desired current carrying capacity of the cable is marked with box 2 and exceeds the inverter output current of 145 A as required in NEK. As the inverter provides three phase power, column three is used. Box three presents the cross section needed to obtain the desired current carrying capacity for a cable installed according to installation method E. The result is a 95 mm^2 aluminium cable with a current carrying capacity of 183 A. For the DC cables connecting the strings and inverters, the same approach is performed by using Table 22. For the inter- building cables, the same approach is performed by using Table 23. Here, installation method D2 is chosen, resulting in a current carrying capacity of 250 A.

Table 21: Current carrying capacity table from NEK 400 for PVC isolated aluminium conductors with a maximum core -and ambient temperature of respectively 70℃ and 30℃

Nominelt leder-tverrsnitt mm²	Flerlederkabler		Énlederkabler				
	To belastede ledere	Tre belastede ledere **1**	To belastede ledere som berører hverandre	Tre belastede ledere forlagt i trekant formasjon	Tre belastede ledere forlagt i flat formasjon		
					Kabler berører hverandre	Kabler forlagt med avstand mellom kablene	
						Horisontalt	Vertikalt
	Metode E	Metode E	Metode F	Metode F	Metode F	Metode G	Metode G
1	2	3	4	5	6	7	8
2,5	23	19,5	–	–	–	–	–
4	31	26	–	–	–	–	–
6	39	33	–	–	–	–	–
10	54	46	–	–	–	–	–
16	73	61	–	–	–	–	–
25	89	78	98	84	87	112	99
35	111	96	122	105	109	139	124
50	135	117	149	128	133	169	152
70 3	173	150 2	192	166	173	217	196
95	210	183	235	203	212	265	241
120	244	212	273	237	247	308	282
150	282	245	316	274	287	356	327
185	322	280	363	315	330	407	376
240	380	330	430	375	392	482	447
300	439	381	497	434	455	557	519
400	–	–	600	526	552	671	629
500	–	–	694	610	640	775	730
630	–	–	808	711	746	900	852

Table 22: Current carrying capacity table from NEK 400 for PVC isolated copper conductors with a maximum core -and ambient temperature of respectively 70°C and 30°C
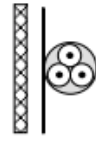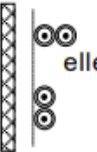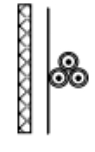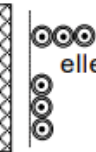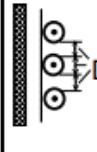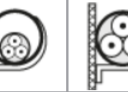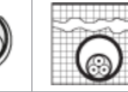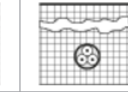
Nominelt leder-tverrsnitt mm²	Referanseinstallasjonsmetode iht. Tabell 52B-1						
	Flerlederkabler		Énlederkabler				
	To belastede ledere	Tre belastede ledere	To belastede ledere som berører hverandre	Tre belastede ledere forlagt i trekant formasjon	Tre belastede ledere forlagt i flat formasjon		
					Kabler berører hverandre	Kabler forlagt med avstand mellom kablene	
						Horisontalt	Vertikalt
	Metode E	Metode E	Metode F	Metode F	Metode F	Metode G	Metode G
1	2	3	4	5	6	7	8
1,5	22	18,5	–	–	–	–	–
2,5	30	25	–	–	–	–	–
4	40	34	–	–	–	–	–
6	51	43	–	–	–	–	–
10	70	60	–	–	–	–	–
16	94	80	–	–	–	–	–
25	119	101	131	110	114	146	130
35	148	126	162	137	143	181	162
50	180	153	196	167	174	219	197
70	232	196	251	216	225	281	254
95	282	238	304	264	275	341	311
120	328	276	352	308	321	396	362
150	379	319	406	356	372	456	419
185	434	364	463	409	427	521	480
240	514	430	546	485	507	615	569
300	593	497	629	561	587	709	659
400	–	–	754	656	689	852	795
500	–	–	868	749	789	982	920
630	–	–	1 005	855	905	1 138	1 070

Table 23: Current carrying capacity table for PVC isolated aluminium conductors with a maximum core -and ambient temperature of respectively 70℃ and 30℃ (Electrcal Installation wiki , 2021).
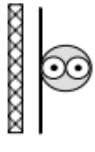
Nominal cross-sectional area of conductors(mm²)	Installation methods of Table B.52.1						
	A1	A2	B1	B2	C	D1	D2
Aluminium							
2.5	14	13.5	16.5	15.5	18.5	18.5	
4	18.5	17.5	22	21	25	24	
6	24	23	28	27	32	30	
10	32	31	39	36	44	39	
16	43	41	53	48	59	50	53
25	57	53	70	62	73	64	69
35	70	65	86	77	90	77	83
50	84	78	104	92	110	91	99
70	107	98	133	116	140	112	122
95	129	118	161	139	170	132	148
120	149	135	186	160	197	150	169
150	170	155	204	176	227	169	189
185	194	176	230	199	259	190	214
240	227	207	269	232	305	218	250
300	261	237	306	265	351	247	282

DC calculations	
I string	6,58
L cable	20
rho cu	0,0175
V mpp min	710
delta V	1 %
S_dc	0,64873239

AC calculations	
I_inv	145
L_cable	40
rho alu	0,0265
V_inv	231
delta_V	1,00 %
S_ac	66,5367965

Inter- building cable, C+B1	
I_tot	1740
L_cable	300
rho alu	0,0265
V	231,213873
delta_V	5,00 %
S_ac	1196,5545
Antall 240 som trengs	4,98564375

Inter- building cable, C+B2	
I_tot	1392
L_cable	148
rho alu	0,0265
V	231,213873
delta_V	5,00 %
S_ac	472,240176
Antall 240 som trengs	1,9676674

Appendix B

String sizing

Module	
P_{nom}	400 W
V_{mpp}	65,8 V
V_{oc}	75,6 V
T_{kVoc}	-0,1768 $\frac{V}{°C}$
T_{kVoc}	-0,234 $\frac{\%}{°C}$
T_{kmpp}	-0,29 $\frac{\%}{°C}$
Width	1,046 m
Length	1,69 m
I_{sc}	6,58 A

Inverter	
P_{nom}	100 kW
V_{max}	1000 V
V_{min}	360 V
I_{max} per MPPT	36 A
$I_{sc\,max}$ per MPPT	50 A
Inputs per inverter	24
MPPTs per inverter	6
Number of inverters	12

Temperatures (°C)	
T_{max}	30
T_{min}	-18
T_{stc}	25
T_{add}	30

The maximum and minimum number of modules per string is calculated to respectively 12 and 7. To determine the maximum number of modules per string, the highest possible open circuit voltage for each module is calculated to 83,2 V

$$V_{OCmax} = V_{OC}\left(1 + \frac{(T_{min} - T_{STC})\,Tk_{Voc}}{100}\right)$$

$$V_{OCmax} = 75,6\,V\left(1 + \frac{(-18 - 25)(-0,234\%)}{100}\right) = 83,2\,V$$

The maximum number of modules per string is then calculated to 12

$$n_{string,max} = \frac{V_{inverter,max}}{V_{OCmax}} = \frac{1000\ V}{83,2\ V} \approx 12$$

The minimum number of modules per string is found by calculating the lowest voltage possible to obtain at maximum power point production. This voltage is found to be 59,1 V and is used further used to calculate the minimum number of modules for each string to be 7.

$$V_{MPmin} = V_{MPP}\left(1 + \frac{(T_{max} + T_{add} - T_{STC})\ Tk_{Vmp}}{100}\right)$$

$$V_{MPmin} = 65,8\ V\left(1 + \frac{(30 + 30 - 25)\ (-0,29\%)}{100}\right) = 59,1\ V$$

$$n_{string,min} = \frac{V_{inverter,min}}{V_{MPmin}} = \frac{360\ V}{59,1\ V} \approx 7$$

Appendix C

Area to be filled with south orientated modules

The row width represents the total space occupied by one tilted module with proper module row spacing to avoid shadowing. The module height difference HD_m and module row spacing S_{mr} is found as these are used to derive the row width W_r. Geometric relationships from Figure 10 is used as a base for these calculations. θ and α respectively corresponds to the module tilt angle and the minimum solar elevation angle.

$$HD_m = Module\ width * \sin(\theta) = 1{,}69m * \sin(40) = 1{,}08m$$

$$S_{mr} = \frac{HD_m}{\tan(\alpha)} = \frac{1{,}08\ m}{\tan(40)} = 1{,}29\ m$$

$$W_r = S_{mr} + [\cos(\theta) * Module\ width] = 1{,}29\ m + [\cos(40) * 1{,}69\ m] = 2{,}58\ m$$

The row with is further used to find the maximal number of modules possible to fit in one column. The column dimensions are presented in Figure 16, and the row length corresponds to the module length, presented in Table 5. The total number of modules to fit in all columns combined is calculated to be 887 after assuming that 5% of the usable roof area disappears due to proper distances to other modules and objects. The total area is to be covered exclusively by modules is eventually found, as this is desired to use for further calculations.

$$Modules\ per\ column = \frac{Column\ width}{Row\ width} * \frac{Column\ length}{Row\ lenght} = \frac{127\ m}{2{,}58\ m} * \frac{14\ m}{1{,}05\ m} * 0{,}95 = 604\ mod$$

$$Total\ modules = Modules\ pr\ column * total\ columns = 590 * 3 = 1813\ modules$$

$$Total\ area = total\ modules * module\ area = 1770 * 1{,}77\ m^2 = 3210\ m^2$$

Area to be filled with east- west modules

$$HD_m = Module\ width * \sin(\theta) = 1,05m * \sin(40) = 0,67\ m$$

$$S_{mr} = \frac{HD_m}{\tan(\alpha)} = \frac{0,67\ m}{\tan(40)} = 0,8\ m$$

$$W_r = S_{mr} + [\cos(\theta) * Module\ width] = 0,8\ m + [\cos(40) * 1,05\ m] = 1,6\ m$$

$$Modules\ per\ column = \frac{Column\ width}{Row\ width} * \frac{Column\ length}{Row\ lenght} = \frac{130\ m}{1,7\ m} * \frac{14\ m}{0,875\ m} * 0,95 = 1155\ mod$$

$$Total\ modules = Modules\ pr\ column * total\ columns = 1075 * 3 = 3465\ modules$$

$$Total\ area = total\ modules * module\ area = 1770 * 1,77\ m^2 = 6134\ m^2$$

Appendix D

Energy production and consumption analysis for the PV system on Coop's roof

Energy consumption and production analysis in kWh

No degradation in year 1. This is the produced energy during the first year. First degradation starts after year 2. Same for power efficiency increase

Year	1	2	3	4	5	6	7	8	9	10	11	12	13	14	15
Consumed energy	2 794 035	2 792 079	2 790 125	2 788 172	2 786 220	2 784 270	2 782 321	2 780 373	2 778 427	2 776 482	2 774 538	2 772 596	2 770 655	2 768 716	2 766 778
Produced PV energy	718 236	715 938	713 647	711 363	709 087	706 818	704 556	702 301	700 054	697 814	695 581	693 355	691 136	688 924	686 720
Energy required from grid	2 075 799	2 076 142	2 076 478	2 076 809	2 077 133	2 077 452	2 077 765	2 078 072	2 078 373	2 078 668	2 078 958	2 079 241	2 079 519	2 079 791	2 080 058

Year	16	17	18	19	20	21	22	23	24	25	26	27	28	29	30	31
Consumed energy	2 764 841	2 762 906	2 760 972	2 759 039	2 757 108	2 755 178	2 753 249	2 751 322	2 749 396	2 747 471	2 745 548	2 743 626	2 741 705	2 739 786	2 737 868	2 735 952
Produced PV energy	684 522	682 332	680 148	677 972	675 802	673 640	671 484	669 335	667 194	665 059	662 930	660 809	658 694	656 587	654 485	652 391
Energy required from grid	2 080 319	2 080 574	2 080 823	2 081 067	2 081 305	2 081 538	2 081 765	2 081 986	2 082 202	2 082 413	2 082 618	2 082 817	2 083 011	2 083 200	2 083 383	2 083 561

Appendix E

Cash flow analysis for the system on Coop's roof

Differences in energy cost with and without PV in NOK

Year	1	2	3	4	5	6	7	8	9	10	11	12	13	14	15
Cost without PV energy	3 026 489	3 025 180	3 023 872	3 022 566	3 021 260	3 019 955	3 018 651	3 017 348	3 016 045	3 014 744	3 013 444	3 012 144	3 010 845	3 009 548	3 008 251
Cost with PV energy	2 545 917	2 546 146	2 546 371	2 546 593	2 546 810	2 547 023	2 547 232	2 547 438	2 547 639	2 547 837	2 548 031	2 548 220	2 548 406	2 548 588	2 548 767
Costs saved from PV produced energy	480 572	479 034	477 501	475 973	474 450	472 932	471 418	469 910	468 406	466 907	465 413	463 924	462 439	460 959	459 484

Cash flow analysis

Year	0	1	2	3	4	5	6	7	8	9	10	11	12	13	14
Cost saved from PV produced energy		480 572	479 034	477 501	475 973	474 450	472 932	471 418	469 910	468 406	466 907	465 413	463 924	462 439	460 959
Mainteinance and reparations		-58000	-58000	-58000	-58000	-58000	-58000	-58000	-58000	-58000	-58000	-58000	-58000	-58000	-58000
Investment cost, PV system	-5 961 160														
Result	-5 961 160	422 572	421 034	419 501	417 973	416 450	414 932	413 418	411 910	410 406	408 907	407 413	405 924	404 439	402 959

Year	16	17	18	19	20	21	22	23	24	25	26	27	28	29	30	31
Cost without PV energy	3 006 955	3 005 660	3 004 366	3 003 073	3 001 781	3 000 489	2 999 199	2 997 909	2 996 621	2 995 333	2 994 046	2 992 760	2 991 475	2 990 191	2 988 908	2 987 625
Cost with PV energy	2 548 941	2 549 112	2 549 279	2 549 442	2 549 601	2 549 757	2 549 909	2 550 057	2 550 201	2 550 342	2 550 479	2 550 613	2 550 743	2 550 869	2 550 992	2 551 111
Costs saved from PV produced energy	458 014	456 548	455 087	453 631	452 179	450 732	449 290	447 852	446 419	444 991	443 567	442 147	440 732	439 322	437 916	436 515

Year	15	16	17	18	19	20	21	22	23	24	25	26	27	28	29	30
	459 484	458 014	456 548	455 087	453 631	452 179	450 732	449 290	447 852	446 419	444 991	443 567	442 147	440 732	439 322	437 916
	-58000	-58000	-58000	-58000	-58000	-58000	-58000	-58000	-58000	-58000	-58000	-58000	-58000	-58000	-58000	-58000
	401 484	400 014	398 548	397 087	395 631	394 179	392 732	391 290	389 852	388 419	386 991	385 567	384 147	382 732	381 322	379 916

Appendix F

Energy production analysis, and cash flow analysis for the systems on C+B1 and C+B2

No degradation in year 1. This is the produced energy during the first year. First degradation starts after year 2. Same for power efficiency increase

Energy consumption and production analysis in kWh, Building 1

Year	1	2	3	4	5	6	7	8	9	10	11	12	13	14	15
Consumed energy	2 794 035	2 792 079	2 790 125	2 788 172	2 786 220	2 784 270	2 782 321	2 780 373	2 778 427	2 776 482	2 774 538	2 772 596	2 770 655	2 768 716	2 766 778
Produced PV energy	1 436 472	1 431 875	1 427 293	1 422 726	1 418 173	1 413 635	1 409 111	1 404 602	1 400 108	1 395 627	1 391 161	1 386 709	1 382 272	1 377 849	1 373 440
Energy required from grid	1 357 563	1 360 204	1 362 831	1 365 446	1 368 047	1 370 634	1 373 209	1 375 771	1 378 319	1 380 855	1 383 377	1 385 887	1 388 383	1 390 867	1 393 338

Year	16	17	18	19	20	21	22	23	24	25	26	27	28	29	30	31
Consumed energy	2 764 841	2 762 906	2 760 972	2 759 039	2 757 108	2 755 178	2 753 249	2 751 322	2 749 396	2 747 471	2 745 548	2 743 626	2 741 705	2 739 786	2 737 868	2 735 952
Produced PV energy	1 369 045	1 364 664	1 360 297	1 355 944	1 351 605	1 347 280	1 342 968	1 338 671	1 334 387	1 330 117	1 325 861	1 321 618	1 317 389	1 313 173	1 308 971	1 304 782
Energy required from grid	1 395 796	1 398 242	1 400 675	1 403 095	1 405 503	1 407 898	1 410 281	1 412 651	1 415 009	1 417 354	1 419 687	1 422 008	1 424 317	1 426 613	1 428 897	1 431 170

Energy consumption and production analysis in kWh, Building 2

Year	1	2	3	4	5	6	7	8	9	10	11	12	13	14	15
Consumed energy	2 794 035	2 792 079	2 790 125	2 788 172	2 786 220	2 784 270	2 782 321	2 780 373	2 778 427	2 776 482	2 774 538	2 772 596	2 770 655	2 768 716	2 766 778
Produced PV energy	1 221 001	1 217 094	1 213 199	1 209 317	1 205 447	1 201 590	1 197 745	1 193 912	1 190 091	1 186 283	1 182 487	1 178 703	1 174 931	1 171 171	1 167 424
Energy required from grid	1 573 034	1 574 985	1 576 925	1 578 855	1 580 773	1 582 680	1 584 576	1 586 461	1 588 335	1 590 199	1 592 051	1 593 893	1 595 724	1 597 544	1 599 354

Year	16	17	18	19	20	21	22	23	24	25	26	27	28	29	30	31
Consumed energy	2 764 841	2 762 906	2 760 972	2 759 039	2 757 108	2 755 178	2 753 249	2 751 322	2 749 396	2 747 471	2 745 548	2 743 626	2 741 705	2 739 786	2 737 868	2 735 952
Produced PV energy	1 163 688	1 159 964	1 156 252	1 152 552	1 148 864	1 145 188	1 141 523	1 137 870	1 134 229	1 130 600	1 126 982	1 123 375	1 119 780	1 116 197	1 112 625	1 109 065
Energy required from grid	1 601 153	1 602 941	1 604 719	1 606 487	1 608 243	1 609 990	1 611 726	1 613 451	1 615 167	1 616 872	1 618 566	1 620 251	1 621 925	1 623 589	1 625 243	1 626 887

Cash flow analysis, C+B1

Year	0	1	2	3	4	5	6	7	8	9	10	11	12	13	14
Cost saved from PV produced energy		1 593 191	1 588 093	1 583 011	1 577 945	1 572 896	1 567 863	1 562 845	1 557 844	1 552 859	1 547 890	1 542 937	1 537 999	1 533 078	1 528 172
Maintenance and reparations		-124 301	-124 301	-124 301	-124 301	-124 301	-124 301	-124 301	-124 301	-124 301	-124 301	-124 301	-124 301	-124 301	-124 301
Rent to building owner		-318 638	-317 619	-316 602	-315 589	-314 579	-313 573	-312 569	-311 569	-310 572	-309 578	-308 587	-307 600	-306 616	-305 634
Investment cost, PV system	-12 430 088														
Result	-12 430 088	1 150 252	1 146 173	1 142 108	1 138 055	1 134 016	1 129 989	1 125 976	1 121 975	1 117 987	1 114 011	1 110 049	1 106 099	1 102 161	1 098 237

Year	15	16	17	18	19	20	21	22	23	24	25	26	27	28	29	30
Cost saved from PV produced energy	1 523 282	1 518 407	1 513 548	1 508 705	1 503 877	1 499 065	1 494 268	1 489 486	1 484 720	1 479 969	1 475 233	1 470 512	1 465 806	1 461 116	1 456 440	1 451 780
Maintenance and reparations	-124 301	-124 301	-124 301	-124 301	-124 301	-124 301	-124 301	-124 301	-124 301	-124 301	-124 301	-124 301	-124 301	-124 301	-124 301	-124 301
Rent to building owner	-304 656	-303 681	-302 710	-301 741	-300 775	-299 813	-298 854	-297 897	-296 944	-295 994	-295 047	-294 102	-293 161	-292 223	-291 288	-290 356
Result	1 094 325	1 090 425	1 086 538	1 082 663	1 078 801	1 074 951	1 071 113	1 067 288	1 063 475	1 059 674	1 055 885	1 052 109	1 048 344	1 044 592	1 040 851	1 037 123

Cash flow analysis, C+B2

Year	0	1	2	3	4	5	6	7	8	9	10	11	12	13	14
Cost saved from PV produced energy		1 354 212	1 349 879	1 345 559	1 341 254	1 336 962	1 332 683	1 328 419	1 324 168	1 319 930	1 315 707	1 311 496	1 307 300	1 303 116	1 298 946
Maintenance and reparations		-98 729	-98 729	-98 729	-98 729	-98 729	-98 729	-98 729	-98 729	-98 729	-98 729	-98 729	-98 729	-98 729	-98 729
Rent to building owner		-270 842	-269 976	-269 112	-268 251	-267 392	-266 537	-265 684	-264 834	-263 986	-263 141	-262 299	-261 460	-260 623	-259 789
Investment cost, PV system	-9 872 858														
Result	-9 872 858	984 641	981 175	977 719	974 274	970 841	967 418	964 006	960 606	957 216	953 837	950 469	947 111	943 764	940 428

Year	15	16	17	18	19	20	21	22	23	24	25	26	27	28	29	30
Cost saved from PV produced energy	1 294 790	1 290 646	1 286 516	1 282 399	1 278 296	1 274 205	1 270 128	1 266 063	1 262 012	1 257 973	1 253 948	1 249 935	1 245 935	1 241 949	1 237 974	1 234 013
Maintenance and reparations	-98 729	-98 729	-98 729	-98 729	-98 729	-98 729	-98 729	-98 729	-98 729	-98 729	-98 729	-98 729	-98 729	-98 729	-98 729	-98 729
Rent to building owner	-258 958	-258 129	-257 303	-256 480	-255 659	-254 841	-254 026	-253 213	-252 402	-251 595	-250 790	-249 987	-249 187	-248 390	-247 595	-246 803
Result	937 103	933 788	930 484	927 191	923 908	920 636	917 374	914 122	910 881	907 650	904 430	901 220	898 020	894 830	891 651	888 482